AD-A121 633 THRESHOLD AND PLASTIC WORK OF FATIGUE CRACK PROPAGATION 1/1
IN HY80 AND HY130 STEELS(U) NORTHWESTERN UNIV EVANSTON
IL DEPT OF MATERIALS SCIENCE M E FINE 01 OCT 82
UNCLASSIFIED N00014-78-C-0565 F/G 11/6 NL

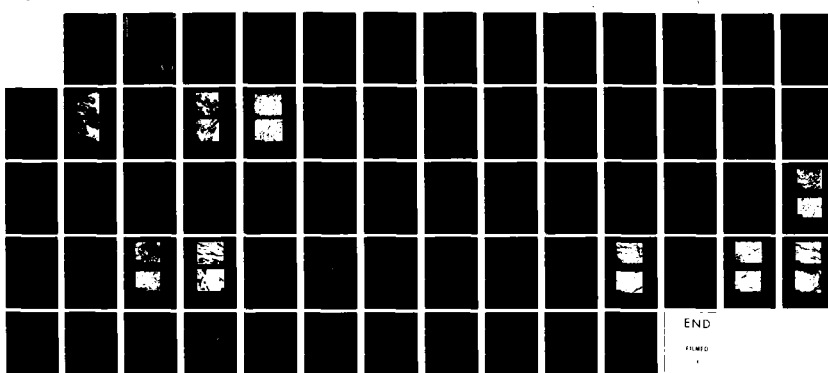

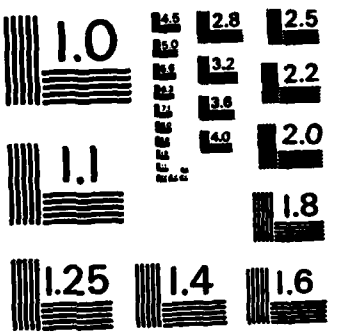

ONR Contract #N00014-78-C-0565

THRESHOLD AND PLASTIC WORK OF FATIGUE CRACK PROPAGATION IN HY80 AND HY130 STEELS

Morris E. Fine, Principal Investigator
Northwestern University
Department of Materials Science and Engineering
Evanston, IL 60201

1 October 1982

Final Technical Report for the period 1 September 1978 - 31 August 1982

Prepared for

Materials and Ceramics Program
Materials Science Division
Office of Naval Research
800 N. Quincy Street
Arlington, Va. 22217

Commanding Officer
Office of Naval Research Branch Office
Rm. 286, 536 S. Clark Street
Chicago, IL 60605

UNCLASSIFIED

SECURITY CLASSIFICATION OF THIS PAGE (When Data Entered)

REPORT DOCUMENTATION PAGE	READ INSTRUCTIONS BEFORE COMPLETING FORM
1. REPORT NUMBER: N00014-78-C-0565	2. GOVT ACCESSION NO.: AD-A121633
3. RECIPIENT'S CATALOG NUMBER	
4. TITLE (and Subtitle): THRESHOLDS FOR FATIGUE INITIATION AND PROPAGATION AND PLASTIC WORK IN HY80 AND HY130 STEELS	5. TYPE OF REPORT & PERIOD COVERED: Final Technical Report 1 Sept 1978 - 31 Aug 1982
	6. PERFORMING ORG. REPORT NUMBER
7. AUTHOR(s): Morris E. Fine	8. CONTRACT OR GRANT NUMBER(s): N00014-78-C-0565
9. PERFORMING ORGANIZATION NAME AND ADDRESS: Northwestern University, Dept. of Materials Science & Engineering, Evanston, Illinois 60201	10. PROGRAM ELEMENT, PROJECT, TASK AREA & WORK UNIT NUMBERS: 122208
11. CONTROLLING OFFICE NAME AND ADDRESS: Metallurgy & Ceramics Program, Mat. Sci. Div., Office of Naval Research, 800 N. Quincy St., Arlington, VA 22217	12. REPORT DATE: October 1, 1982
	13. NUMBER OF PAGES: 62
14. MONITORING AGENCY NAME & ADDRESS (if different from Controlling Office): Commanding Officer, Office of Naval Research Branch Office, Rm. 286, 536 S. Clark Street, Chicago, Illinois 60605	15. SECURITY CLASS. (of this report): Unclassified
	15a. DECLASSIFICATION DOWNGRADING SCHEDULE

16. DISTRIBUTION STATEMENT (of this Report)

Distribution is Unlimited

17. DISTRIBUTION STATEMENT (of the abstract enters .n Block 20, if different from Report)

18. SUPPLEMENTARY NOTES

19. KEY WORDS (Continue on reverse side if necessary and identify by block number)

HY80, HY130, fatigue crack propagation, threshold

20. ABSTRACT (Continue on reverse side if necessary and identify by block number)

The fatigue crack propagation rate da/dN in the near threshold stress intensity range (ΔK) and mid-ΔK range were investigated for HY80 and HY130 with various heat treatments. With the standard heat treatments, the threshold stress intensity range ΔK_{th} for HY80 is higher, 4.2 $MN/m^{\frac{3}{2}}$, than for HY130, 3.8 $MN/m^{\frac{3}{2}}$. For HY80 dual phase heat treatments increased ΔK_{th} considerably to 5.4 $MN/m^{\frac{3}{2}}$. No heat treatment was found which increased ΔK_{th} of HY130. In the mid-ΔK range da/dN for a given ΔK is smaller for HY80 with standard heat treatment than for HY130 with

DD FORM 1 JAN 73 1473 EDITION OF 1 NOV 65 IS OBSOLETE

UNCLASSIFIED

SECURITY CLASSIFICATION OF THIS PAGE (When Data Entered)

20. continued

standard heat treatment. This is due to a larger plastic work of fatigue crack propagation U in the HY80. No heat treatments were found which decreased da/dN in HY130. The theoretical equation $da/dN = A(\Delta K)^4/\mu\sigma_y^2 U$ where A is a universal constant near 4×10^{-3}, μ is the shear modulus and σ_y is the cyclic 0.2% offset yield stress has been shown to hold for HY80 and HY130.

PERSONNEL

Dr. Morris E. Fine, Walter P. Murphy Professor of Materials Science and Engineering, Principal Investigator

Dr. Sook-In Kwun, Postdoctorate Research Associate, Department of Materials Science and Engineering, 9/1/78 to 8/8/79 half-time, 7/15/80 to 8/31/80 half-time. Present address: Department of Metallurgical Engineering, Korea University, Anam-Dong, Sungbuk-ku, Seoul, Korea

Mr. Jain-Long Horng, Graduate Research Assistant, Department of Materials Science and Engineering, 9/1/79 to termination of contract (8/31/82)

INTRODUCTION

The propagation of macro-fatigue cracks is usually divided into three stages: a) the near threshold region where the rate of fatigue crack propagation $\frac{da}{dN}$ increases very rapidly with an increase in stress intensity range, ΔK, from a threshold value, ΔK_{th}, b) the mid-region where the Paris relation $\frac{da}{dN} = C(\Delta K)^m$ is followed; C and m are considered to be constants for a given material, and c) the region of growth to final failure where K_{max} approaches K_c.

The objective of the present research was to make a comprehensive study of the effect of heat treatment and microstructure on the fatigue crack propagation rate from the threshold stress intensity (ΔK_{th}) to the mid-range of stress intensity in HY80 and HY130. It was hoped that such a study would lead to an improvement in fatigue properties of HY80 and HY130 as well as a better understanding of how fatigue crack propagation is related to microstructure. While there is little theory for ΔK_{th}, the mid-region of ΔK is relatively well understood. In previous research in this laboratory, the plastic work required to propagate a unit area of fatigue crack U was shown to be an important parameter for controlling the rate of fatigue crack propagation; $\frac{da}{dN}$ is inversely proportional to U. A technique was developed for measuring U by cementing foil strain gages ahead of propagating fatigue cracks and mapping the local plastic work over the plastic zone at the crack tip.[1,2,3]

Many theoretical and empirical equations for fatigue crack propagation in the mid-range can be reduced to the approximate form[2,3]

$$\frac{da}{dN} = A \frac{(\Delta K)^4}{\mu\sigma^2 U} \qquad (1)$$

where a is the crack length, N is the cycle number, ΔK is the stress intensity amplitude, μ is the shear modulus, σ is the appropriate cyclic flow stress, U is the plastic work required for a unit area of fatigue crack propagation and A is a dimensionless constant whose value will be discussed later. The 0.2% cyclic yield stress σ_y' is used for σ since the metal at the crack tip has been cyclically strained. Weertman[4] proposed that when $m = 4$, U is independent of ΔK but when m is less than 4, U is a function of ΔK according to the equation

$$U = B(\Delta K)^n \tag{2}$$

with $n = 4-m$. This was experimentally verified.[3]

Equation (1) tells us that in order to decrease da/dN at a given value of ΔK the yield stress must be increased without decrease in U or U must be increased keeping yield stress constant.

From a practical point of view, the near-threshold region of ΔK is more important than the mid-ΔK region because after a fatigue crack has initiated and grown to a macro-size (i.e., a few grain diameters) most of the fatigue lifetime has been expended. Mid ΔK fatigue crack growth is too near final failure.

Based on the idea that the threshold stress intensity for propagation of a macro-fatigue crack ΔK_{th} is determined by the stress necessary to operate a dislocation source near the tip of the fatigue crack, the following simple expression was derived[5] for low $R(\sigma_{min}/\sigma_{max})$ values,

$$\Delta K_{th} = \alpha \sigma_s (2\pi s)^{\frac{1}{2}} \tag{3}$$

where σ_s is the stress necessary to operate the dislocation source, s is

the distance from the crack tip to the dislocation source, and α is a factor which takes account of the fact that plasticity reduces the stress in the plastic zone from that calculated from fracture mechanics. Variation of ΔK_{th} with temperature in some aluminum alloys was tentatively explained by this theory.[6] Since α, σ_s, and s depend on microstructure, a dependence of ΔK_{th} on microstructure can be explained.

Hornbogen et al.[7] suggested that the near threshold fatigue crack propagation rate is low if extensive reversible dislocation motion occurs at the crack tip, i.e., few slip steps form and few dislocations accumulate. Lindigkeit et al.[8] were able to explain their data on Al alloys on this basis. Again a dependence on microstructure is predicted.

Besides the great importance of HY80 and HY130 as pressure vessel steels and the desirability for improving their fatigue resistance, they appeared to be good candidates for study of the role of microstructure in determining fatigue crack propagation because a very large variety of structures may be produced. For example, because of the secondary hardening characteristics of HY130, a variety of structures may be produced all having the same yield strength. Further, HY80 may be heat treated to have a dual martensite-ferrite structure. McEvily[9] has shown that such structures give very high values of ΔK_{th} in 1018 steel.

ALLOYS STUDIED

For this research HY80 and HY130 of the compositions shown in Table 1 in weight percent, were obtained from the U. S. Steel Research Laboratory courtesy Dr. L. F. Porter.

Table 1. Compositions of HY80 and HY130 Studied

	C	Ni	Cr	Mo	Mn	V	Si
HY80	0.18	3.00	1.58	0.50	0.32	0.006	0.27
HY130	0.10	5.33	0.49	0.57	0.35	0.064	0.23

The standard heat treatments for these are: HY80, austenitized at 900° C and tempered 1 hr at 700° C; HY130, austenitized at 815° C and tempered 1 hr at 610° C.

PLASTIC WORK OF FATIGUE CRACK PROPAGATION (MID-ΔK REGION) IN HY80 AND HY130

The first experiment conducted[10] was to measure the plastic work per unit area of fatigue crack propagation U in Eq.(1) for both HY80 and HY130 with standard heat treatment. As subsequently discussed, the value of U for HY80 is more than three times larger than for HY130 in keeping with the higher fatigue crack propagation rate in the latter.

Knowing U, μ, σ_y', the constant A in Eq.(1) was calculated. Its value for HY80 and HY130 is nearly identical to that for other steels. This was an important confirmation of Eq.(1).[2] For this research, panel specimens, 3.5 mm x 25 mm x 100 mm, were machined so that the rolling direction was parallel to the long direction which was also the stress direction. Specimens for determining cyclic stress-strain curves were prepared with gage sections 7.8 mm long and 4.0 mm wide. After machining, the austenitizing was done in argon and the tempering in a salt bath, as described in Table 1. After heat treatment, the flat surfaces of the specimens were polished through 0.05 μm alumina powder and then a 3 mm x 0.2 mm center notch was introduced using electro-discharge machining with a thin Cu plate electrode.

The fatigue crack propagation rate measurements were performed at constant load range, ΔS, on a closed loop MTS machine under load control using a sinusoidal wave of 30 or 50 Hz with R = 0.05. Laboratory air of 47%

relative humidity and dry argon environments were employed. The crack ends were followed using a 40X traveling microscope.

For the Paris relation range of ΔK the details for measuring and calculating the plastic work per unit area of fatigue crack propagation, U, are described fully.[1,2,3] The measurements, using small strain gages (Micro-measurements MA-06-008CL-120) cemented astride and above the expected crack path, were done at constant ΔK in dry argon at R = 0.05 and a frequency of 30 Hz. The stress intensity range, ΔK, was kept constant by decreasing ΔS every 100 μm increase in crack length.

For determination of U, a set of hysteresis loops for fully reversed strain amplitude are needed. These were obtained by both the incremental step and multiple 30 cycle block step tests which also gave cyclic stress-strain curves and σ_y'.

Foils for studying the structure in the plastic zone using TEM were prepared by cutting sections, approximately 300 μm thick including and parallel to the crack plane, using a low speed saw. The sections were first briefly electropolished on the fracture surface side to remove 3 to 4 μm with the saw cut surface covered with "stopper". The "stopper" was then removed from the saw cut surface and painted onto the fracture surface. Electropolishing of the saw cut surface was continued until the foil was approximately 80 μm thick. Finally, the sections were thinned from the same side in a jet thinning machine using 15% HNO_3 solution. The final foils were approximately 10-20 μm from the fracture surface. For comparison, foils were also taken from outside the plastic zone. The foils were observed under an Hitachi HU-200F TEM at 200 kV. The fatigue fracture surfaces were also investigated with a JEOL JSM-50A scanning microscope at 25 kV. In all cases the TEM and SEM studies were on specimens where the fatigue crack

propagation had been carried out at a constant ΔK of 20 $MN/m^{\frac{3}{2}}$.

The cyclic stress-strain curves are shown in Fig. 1. Data for 4140 steel quenched and tempered at 650° C are shown for comparison. Both HY80 and HY130 steels showed cyclic softening, i.e., the cyclic stress-strain curves are below the monotonic curves. This behavior is typical of quenched and tempered steels such as 4140 tempered at 650° C. The large amount of cyclic softening at small strain ranges suggests a large contribution to cyclic softening from mechanical unpinning of dislocations. The cyclic stress-strain curves obtained by the multiple step test are shown by the points and these are very close to the curves determined by incremental step tests in both steels. In the multiple step tests, the strain amplitude is increased in steps after 30 cycles at each amplitude. The plastic strains, i.e., widths of the hysteresis loops at the same total strain for the two kinds of tests, were also compared and will be discussed later. The monotonic and cyclic mechanical properties of the two HY steels are listed in Table 2. While HY130 is much stronger than HY80, the ratios of cyclic to monotonic 0.2% offset yield strength are the same.

Table 2. Mechanical Properties and ΔK_{th} Values of HY80, HY130, and 4140 (650° C T) Steels

	HY80	HY130	4140 (650° C temper)
Monotonic 0.2% yield strength (σ_y)	626 MN/m^2	1042 MN/m^2	883 MN/m^2
Cyclic 0.2% yield strength (σ_y')	521 MN/m^2	868 MN/m^2	555 MN/m^2
Young's modulus (E)	1.96×10^5 MN/m^2	1.96×10^5 MN/m^2	2.10×10^5 MN/m^2
Monotonic strain hardening exponent (η)	0.041	0.030	0.012
Cyclic strain hardening exponent (η')	0.129	0.103	0.196
σ_y'/σ_y	0.83	0.83	0.63
ΔK_{th}	4.2 $MN/m^{\frac{3}{2}}$	3.8 $MN/m^{\frac{3}{2}}$	3.5 $MN/m^{\frac{3}{2}}$

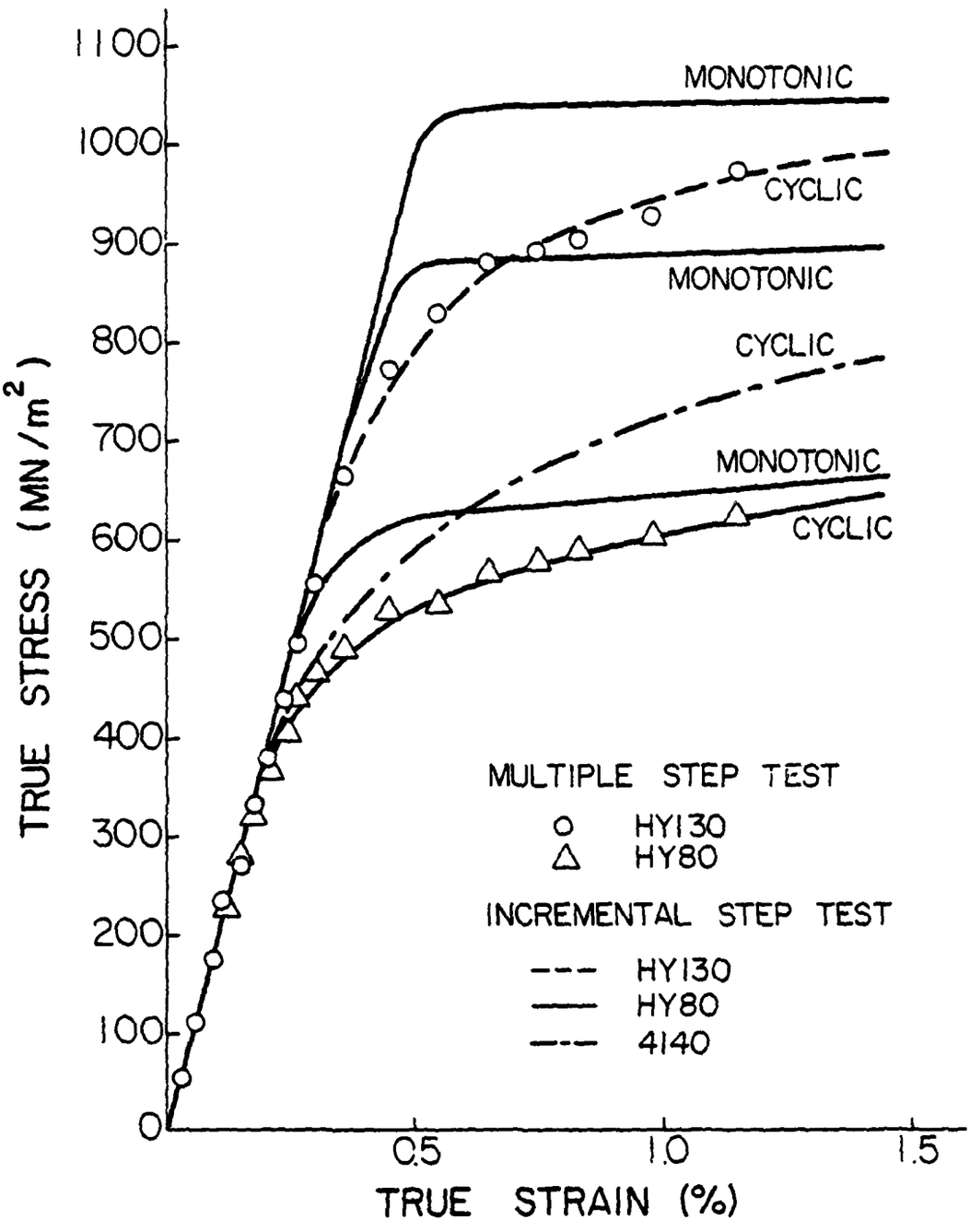

Figure 1. Monotonic and cyclic stress-strain curves for 4140 (650°C temper), HY80 and HY130 steels.

In the determination of U, the first step is the determination of the local hysteretic plastic work density, U_{XY}, for coordinates X and Y in the plastic zone determined as described in the references.[1-3] These are plotted against X, the distance from the crack tip to the center of strain gage and Y, the distance between crack plane and the foil strain gage in Fig. 2 to give a map of one-half of the plastic zone. Integration over all X and Y gives U. The value of U for HY80 at ΔK of 20 $MN/m^{\frac{3}{2}}$ is 3.5 times larger than that for HY130 (7.7×10^5 vs. 2.2 J/m^2) as shown in Table 3. As shown in Fig. 2, HY80 has a $2\frac{1}{2}$ times bigger plastic zone than HY130 because of its lower yield stress.

Table 3. Values of Quantities in Equation (1) for HY80 and HY130

	σ_y' (MN/m^2)	$\Delta K_{\frac{3}{2}}$ ($MN/m^{\frac{3}{2}}$)	$\left.\frac{da}{dN}\right\|_{\Delta K=20\ MN/m^{\frac{3}{2}}}$ (m/cycle)	U (J/m^2)	A
HY80 (700° C temper)	521	20	3.5×10^{-8}	7.7×10^5	3.6×10^{-3}
HY130 (610° C temper)	868	20	5.0×10^{-8}	2.2×10^5	4.0×10^{-3}

Atmosphere: Dry argon

The high tempering temperature (700° C) for HY80 results in a very much "recovered" microstructure. The location of the original martensite laths are not evident as shown in Fig. 3(a) and the density of dislocations is quite low. Large globular cementite particles are present. The structure inside the plastic zone some 10-20 μm from the fracture surface, as illustrated by Fig. 3(b), has been changed by the cyclic plastic deformation to consist of very well defined dislocation cells. As it is well known, ferritic steels form dislocation cells by fatigue cycling in the high plastic strain range. On the other hand, the tempering effect in HY130 is not as advanced as in

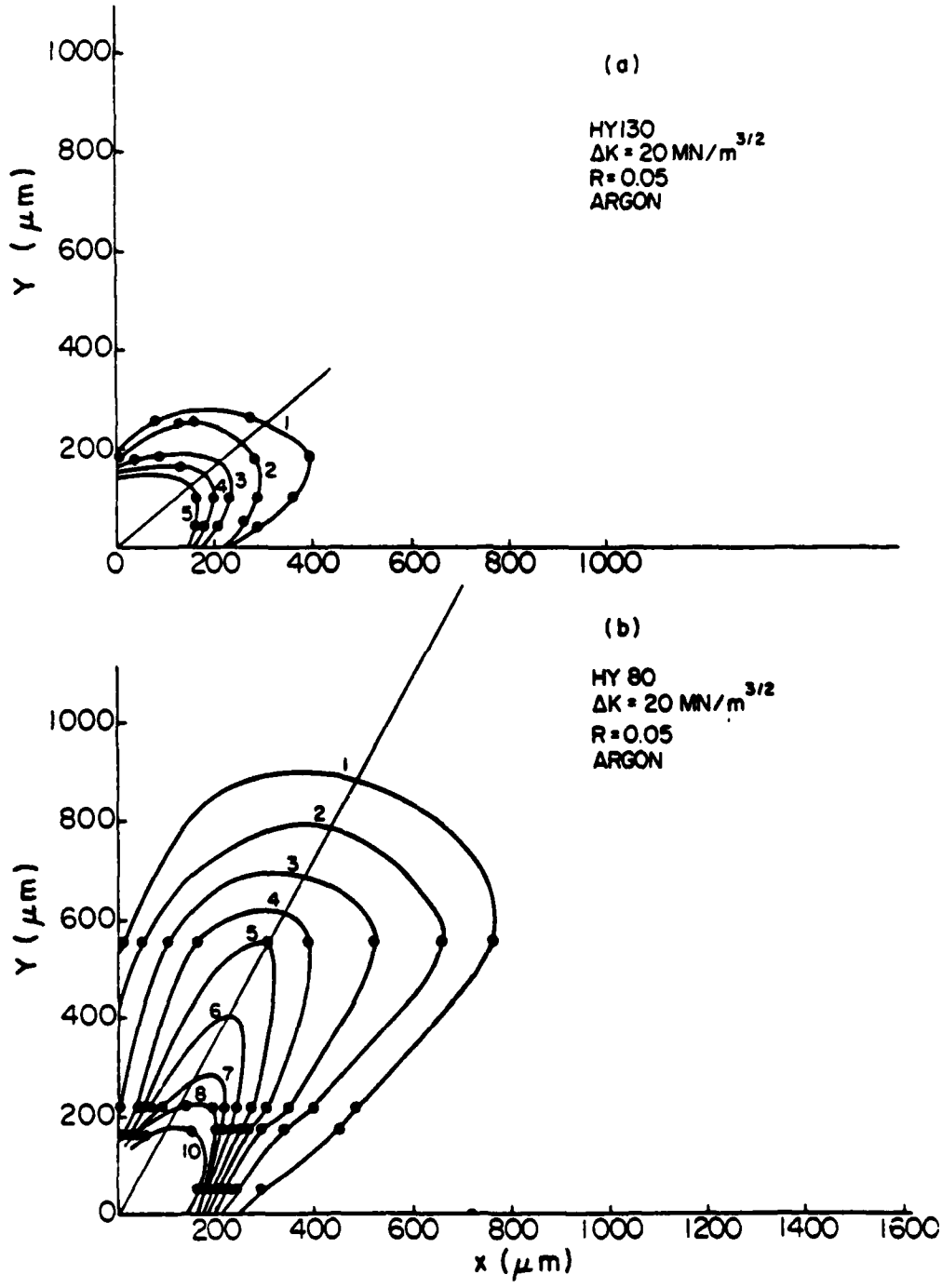

Figure 2. Local plastic work density contour lines versus distance from crack tip: (a) HY80, (b) HY130. Units are 10^{11} J/m^{-4}.

(a)

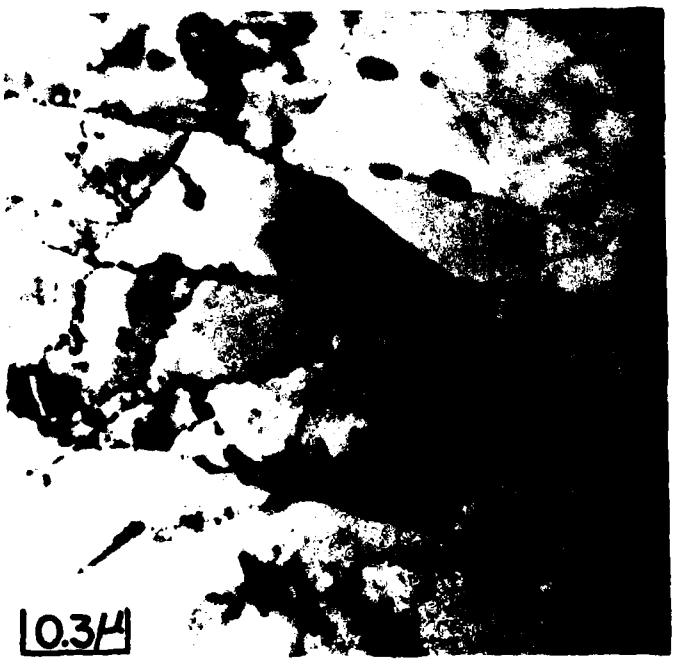

(b)

Figure 3. Transmission electron micrographs of HY80 and HY130 steel

(a) HY80 as heat treated condition

(b) HY80 inside plastic zone after cycling at $\Delta K = 20$ MN/m$^{\frac{3}{2}}$

HY80, as shown in Fig. 3(c). This must be due mainly to the lower tempering temperature of 610° C, but V also retards tempering. A lath structure is observed with a high density of dislocations. A few globular cementite particles are seen mainly on lath boundaries. Very fine VC particles are seen in both Figs. 3(c) and 3(d). The microstructure of the plastic zone for HY130 did not show much difference from the as heat treated condition; a high dislocation density was still retained and there were no apparent dislocation cells. All plastic zones of Fig. 3 were developed at ΔK equal to 20 $MN/m^{\frac{3}{2}}$.

The fatigue fracture surfaces at $\Delta K = 20$ $MN/m^{\frac{3}{2}}$ for the two steels were examined. The SEM micrographs of both HY80 and HY130 in Fig. 4 showed transgranular fracture, quasi-cleavage and secondary cracks. However, the fracture surface of HY80 was somewhat rougher indicating a more ductile fracture process. Striation-like features were seen on the fracture surfaces of both steels with larger spacing for HY130 which has the higher da/dN. However, these spacings were almost ten times the da/dN values measured in both HY80 and HY130 steels at 20 $MN/m^{\frac{3}{2}}$.

Discussion

A number of researchers have reported that $da/dN|_{\Delta K}$ in steels is approximately independent of alloying and heat treatment.[11] The origin of this effect according to Eq.(1) lies in an inverse dependence between the strength of the steel and U. High strength alloys have small plastic zones at a given ΔK and this usually gives low U values. Recall that U is obtained by integrating the local plastic work density over the plastic zone. However, a number of exceptions to the inverse relation between yield strength and U have been observed. Lowering the C content and tempering temperature, keeping strength essentially constant, resulted in lower $da/dN|_{\Delta K}$ and correspondingly

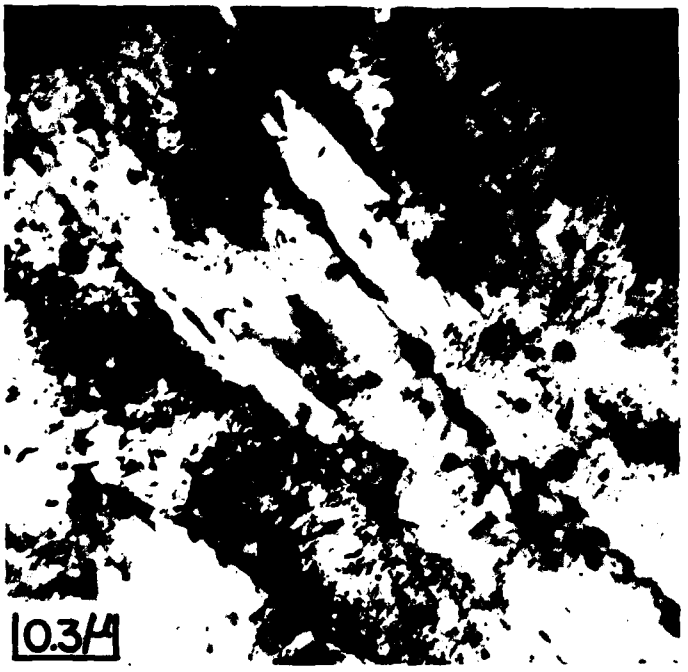

(c)

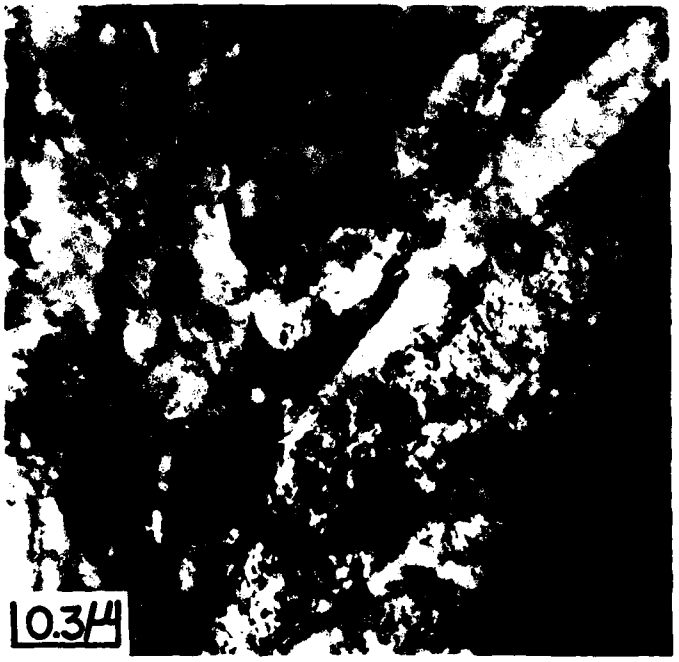

(d)

Figure 3. (c) HY130 microstructure of as heat treated condition
(d) HY130 microstructure within the plastic zone

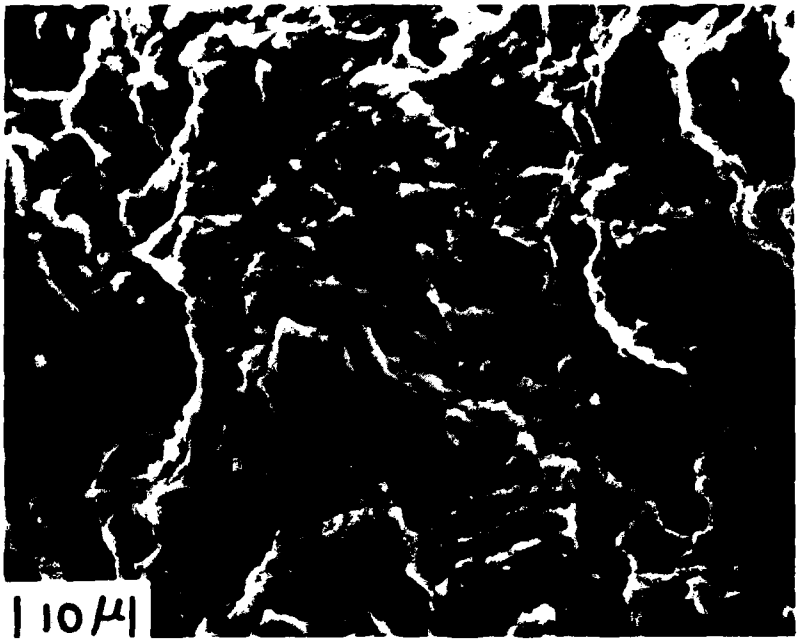

Figure 4. Scanning electron micrograph of the fatigue fracture surfaces of HY80 and HY130 steels in argon at $\Delta K = 20$ MN/m$^{3/2}$

(a) HY80 (b) HY130

larger U.[12] In Nb-bearing HSLA steel, quenching and tempering to give secondary hardening due to coherent NbC precipitates causes high da/dN and lower U[13] where tempering at a lower temperature resulted in a much higher U and much lower da/dN at 20 $MN/m^{\frac{3}{2}}$ with only a small decrease in σ_y'.

In the present study, HY80, which has the higher C content and higher tempering temperature and lower strength, has 3.5 times larger U than HY130. However, the U value for the Nb-HSLA steel tempered at 400° C has a four times larger U than HY80 even though σ_y' is higher for the former, further demonstrating the importance of the microstructure in determining U and $da/dN|_{\Delta K}$. It appears that the heat treatments which give rise to secondary hardening from VC or NbC precipitates reduce U and increase da/dN. This may be due to coherent NbC or VC precipitates being sheared or disordered by the to and fro movement of dislocations during fatigue leading to strain localization and thereby easy crack propagation. Thus, the lower U for HY130 may result not only from higher strength but also from strain localization due to VC precipitates. Easier cross slip of dislocations for HY80 is indicated by the formation of dislocation cells during cycling. Thus HY80 is able to accommodate larger amounts of plastic strain. The larger cyclic ductility, i.e., higher U, for HY80 is also seen from the fracture surfaces.

According to Rice[14], the cyclic plastic zone size can be calculated by the equation

$$r_p = \frac{\pi}{32}\left(\frac{\Delta K}{\sigma}\right)^2 \qquad (4)$$

where r_p is the plastic zone size and σ is often taken to be the 0.2% offset yield strength, σ_y'. Izumi and Fine[15] showed that when σ in Eq.(4) is replaced by the stress at which hysteresis loops are first observed,

Eq.(4) predicts the strain gage measured value of plastic zone size rather well. The measured plastic zone sizes for HY80 and HY130 for a ΔK of 20 $MN/m^{\frac{3}{2}}$ along the direction of the lightly drawn straight lines in Fig. 3 were 1050 and 410 μm, respectively. These sizes are 7 to 8 times larger than those calculated from Eq.(4) with σ_y' substituted for σ.

The material in front of a propagating fatigue crack undergoes cyclic plastic deformation in a similar way to the multiple step test sample where the strain amplitude is controlled for a block of cycles, 30 in the present experiments, and then increased to the next value. Hysteresis was first noted at the strain amplitude corresponding to 175 MN/m^2 stress amplitude for HY80 and 270 MN/m^2 for HY130. Both are nearly one-third of σ_y'. When these values are substituted for σ into Eq.(4) the calculated plastic zone sizes are 1280 μm for HY80 and 539 μm for HY130 which are in relatively good agreement with the measured values. It should be noted that the above stresses are considerably below the published values of endurance limit[16] which for HY130 is approximately 575 MN/m^2.

The values of A, 3.6 and 4.0×10^{-3} are close to that found previously[2] for low C steel 4.3×10^{-3} even though the U value is an order of magnitude greater.

From the point of view of utilizing HY130, while it has a higher strength than HY80 the fatigue crack propagation rate at a given value of ΔK is higher. Thus for applications where the fatigue crack propagation rate is the critical design parameter HY80 is preferred.

Equation (1) indicates some research directions for decreasing $(da/dN)_{\Delta K}$ by attempting to change the microstructure. This is the subject of the next section of this report.

EFFECT OF HEAT TREATMENT ON FATIGUE CRACK PROPAGATION RATE OF HY130 IN MID-ΔK REGION

Since the fatigue crack propagation rate of HY130 is considerably faster than that of HY80 due to the lower value of U, a series of experiments with HY130 were initiated to determine whether an improvement could be achieved by changing the heat treatment.

Previously, Kwun and Fournelle[13] who studied a 0.034Nb-0.08C steel found that tempering at 400° C (5 hrs) rather than 550° C (10 hrs) resulted in a four times greater value of U even though the yield strengths were about the same. These authors proposed that the difference arises from a difference in composition and morphology of the carbide phase although this was not investigated.

Since HY130 contains V (0.064 wt.%) and C (0.10 wt.%), it was thought that similar results to the Nb steel might be obtained. Since Eq.(1) has been shown to hold at least as a good first approximation, it was decided to measure da/dN vs. ΔK in the mid-ΔK region and use Eq.(1) to give an indication of how U changed with heat treatment.

The standard heat treatment for HY130 is austenitizing at 815° C followed by tempering 1 hr at 610° C. After quenching from 815° C, there was no evidence for undissolved VC when specimens were examined at 1000 magnification in the optical microscope; therefore, an austenitizing temperature of 815° C was selected for the study. Samples were first austenitized at 815° C in argon, water quenched and then tempered for various times at 400, 500, and 650° C. Rockwell C hardness versus tempering time is shown in Fig. 5. The hardness falls off more rapidly with time, of course, as the tempering temperature is increased; however, there is some evidence for secondary hardening on tempering at 550° C, no doubt due to VC replacing Fe_3C. Four

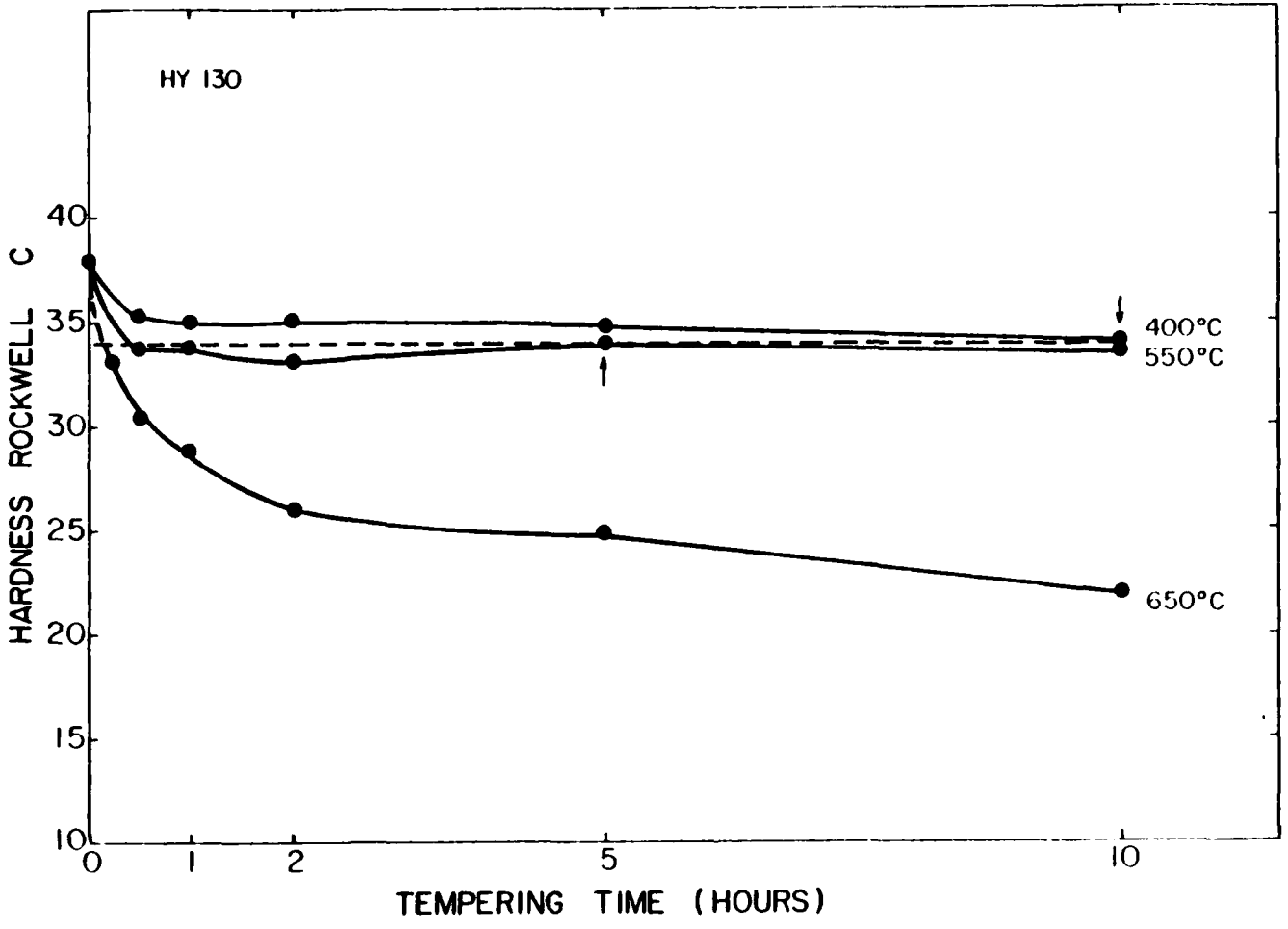

Figure 5. Rockwell C hardness of HY130 austenitized at 815° C and tempered at the temperatures indicated.

tempering treatments giving approximately the same Rockwell C hardness were chosen.

A	10 hrs at 400° C
B	5 hrs at 550° C
C	$\frac{1}{4}$ hr at 650° C
D	1 hr at 610° C (standard treatment)

As previously da/dN was measured versus ΔK in panel specimens 100 mm by 3.5 mm by 25 mm containing a 3 mm by 0.2 mm center notch introduced by spark machining. All heat treatments were done after specimen preparation but before spark machining. The crack lengths were measured with a 40X telemicroscope. The results for 55% relative humidity air and dry argon are shown in Figs. 6, 7, 8 and 9. The results for argon were all somewhat lower than those in air, particularly for the 400° C tempered specimens at low ΔK and 610° C tempered specimen at high ΔK. There was, however, no dramatic difference in the da/dN curves for the four heat treatments as with the Nb steel. Table 4 compares the results at ΔK = 15, 20 and 30 $MN/m^{\frac{3}{2}}$. The coefficients of C and m in the Paris equation, $da/dN = C(\Delta K)^m$, are also listed.

The absence of a large effect of heat treatment on da/dN keeping hardness constant in the mid-ΔK region in HY130, as observed in the 0.034 wt.% Nb-0.08 wt.% C steel[13], was disappointing and means that U is approximately the same for all of the heat treatments studied. Since the Paris exponent is near 3, U is predicted to vary somewhat with ΔK.

The environmental effect of 55% R.H. air compared to argon was found to be small too, but the values of da/dN in air were always higher.

Because further research along these lines appeared to be unprofitable, it was dropped in favor of study of the near threshold stress intensity region of ΔK where microstructure has been shown to have a large effect.

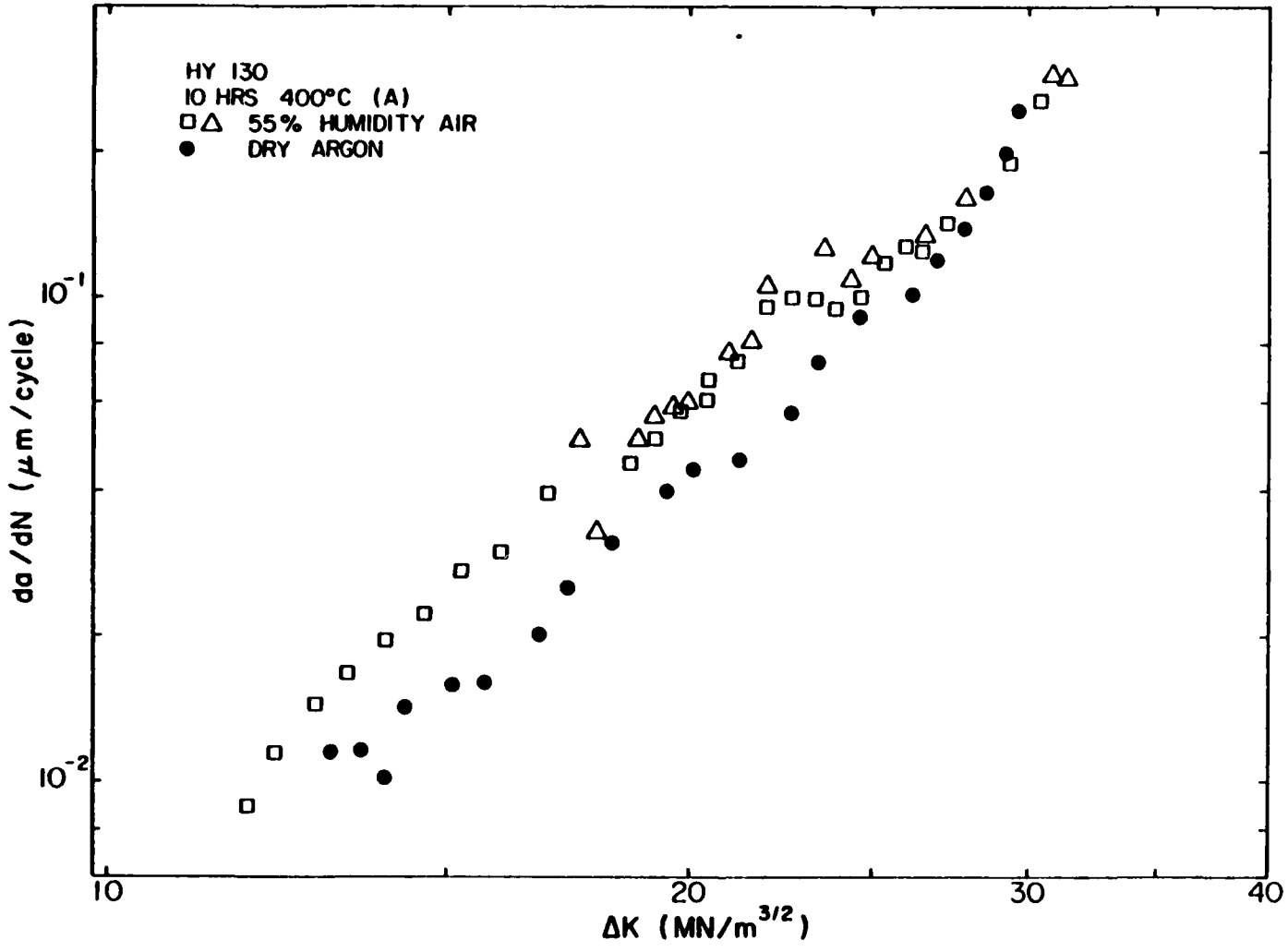

Figure 6. Fatigue crack propagation rate versus ΔK of HY130 austenitized at 815° C and tempered 10 hrs at 400° C.

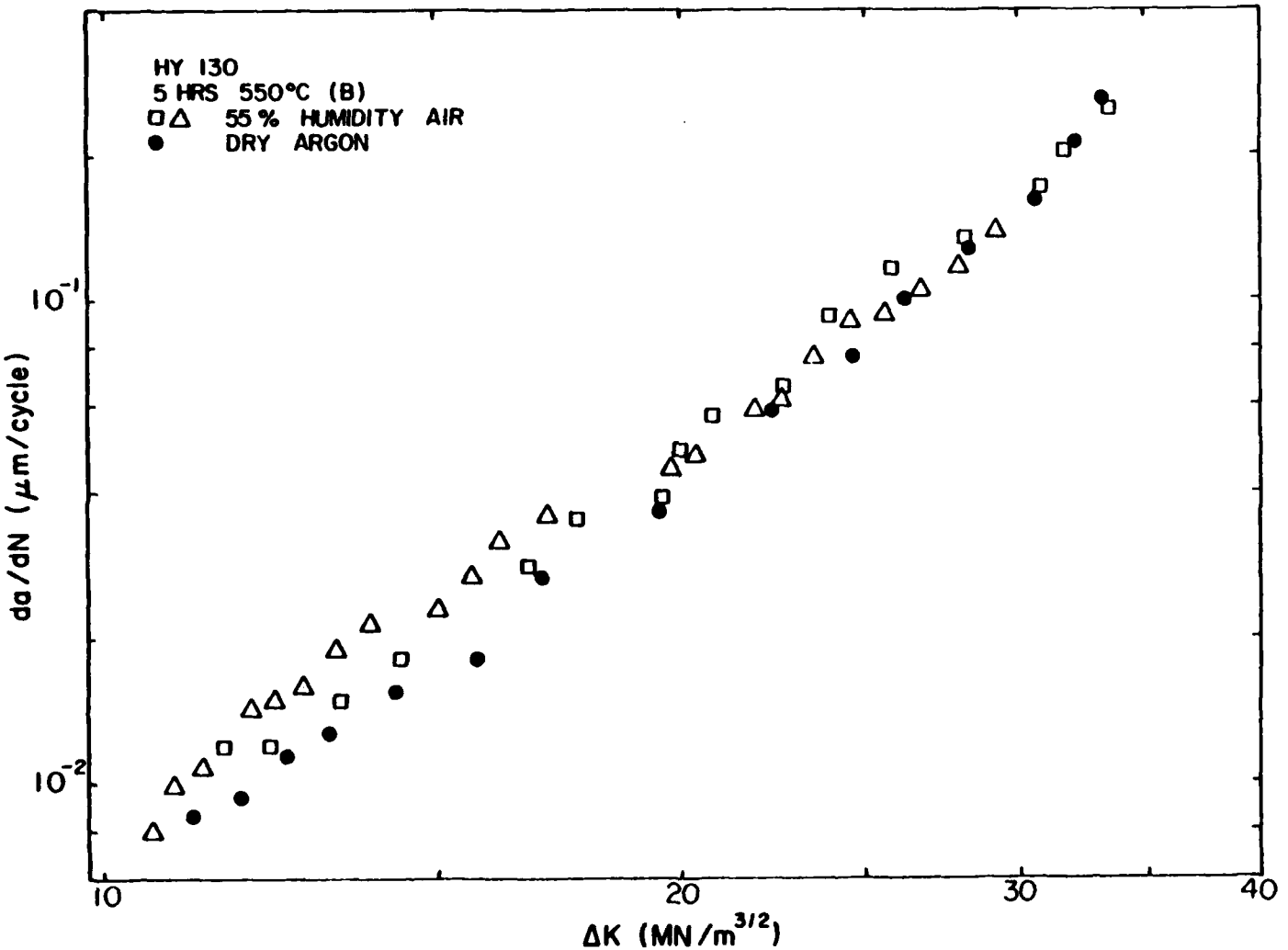

Figure 7. Fatigue crack propagation rate versus ΔK of HY130 austenitized at 815°C and tempered 5 hrs at 550°C.

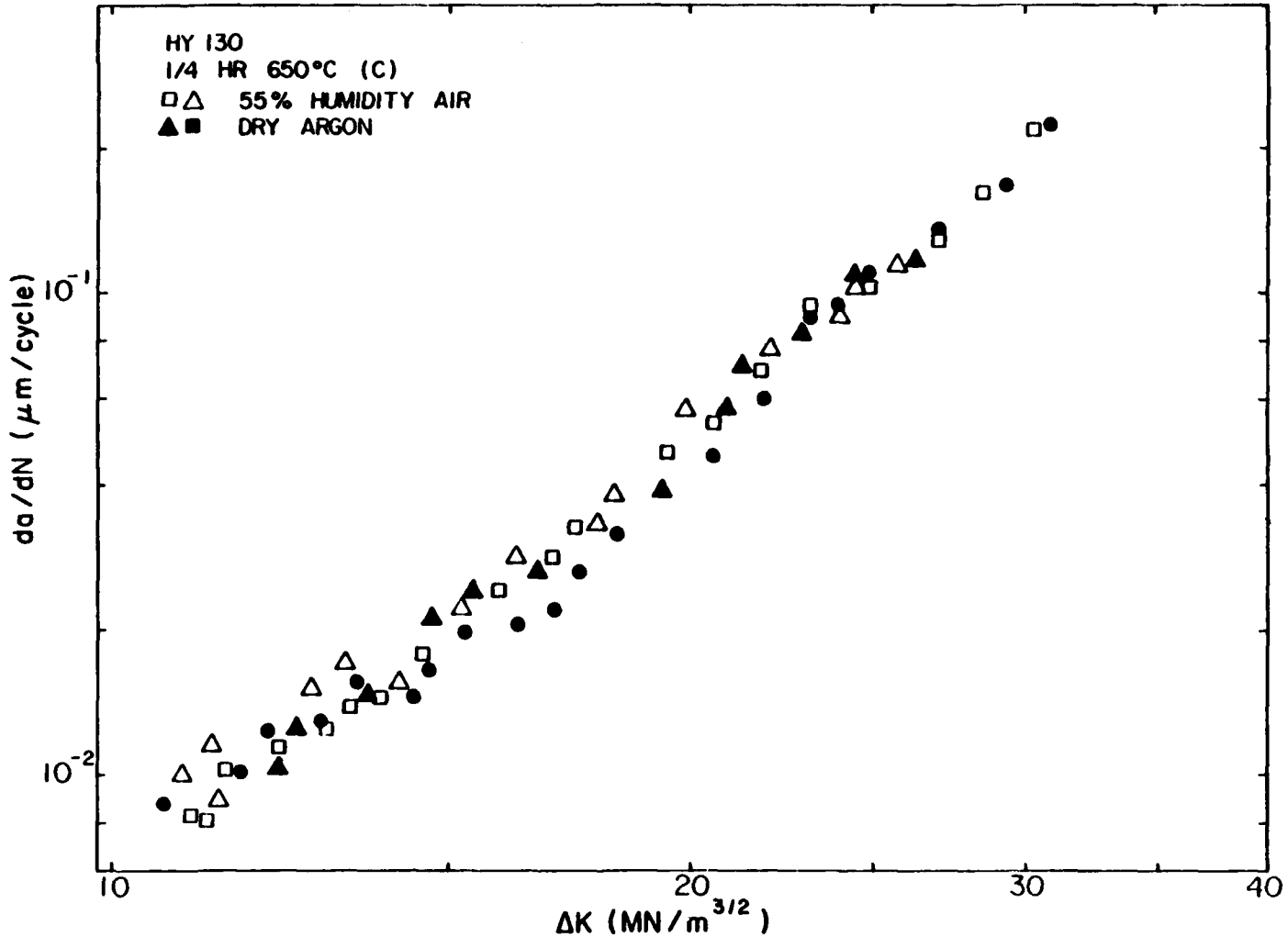

Figure 8. Fatigue crack propagation rate versus ΔK of HY130 austenitized at 815° C and tempered $\frac{1}{4}$ hr at 650° C.

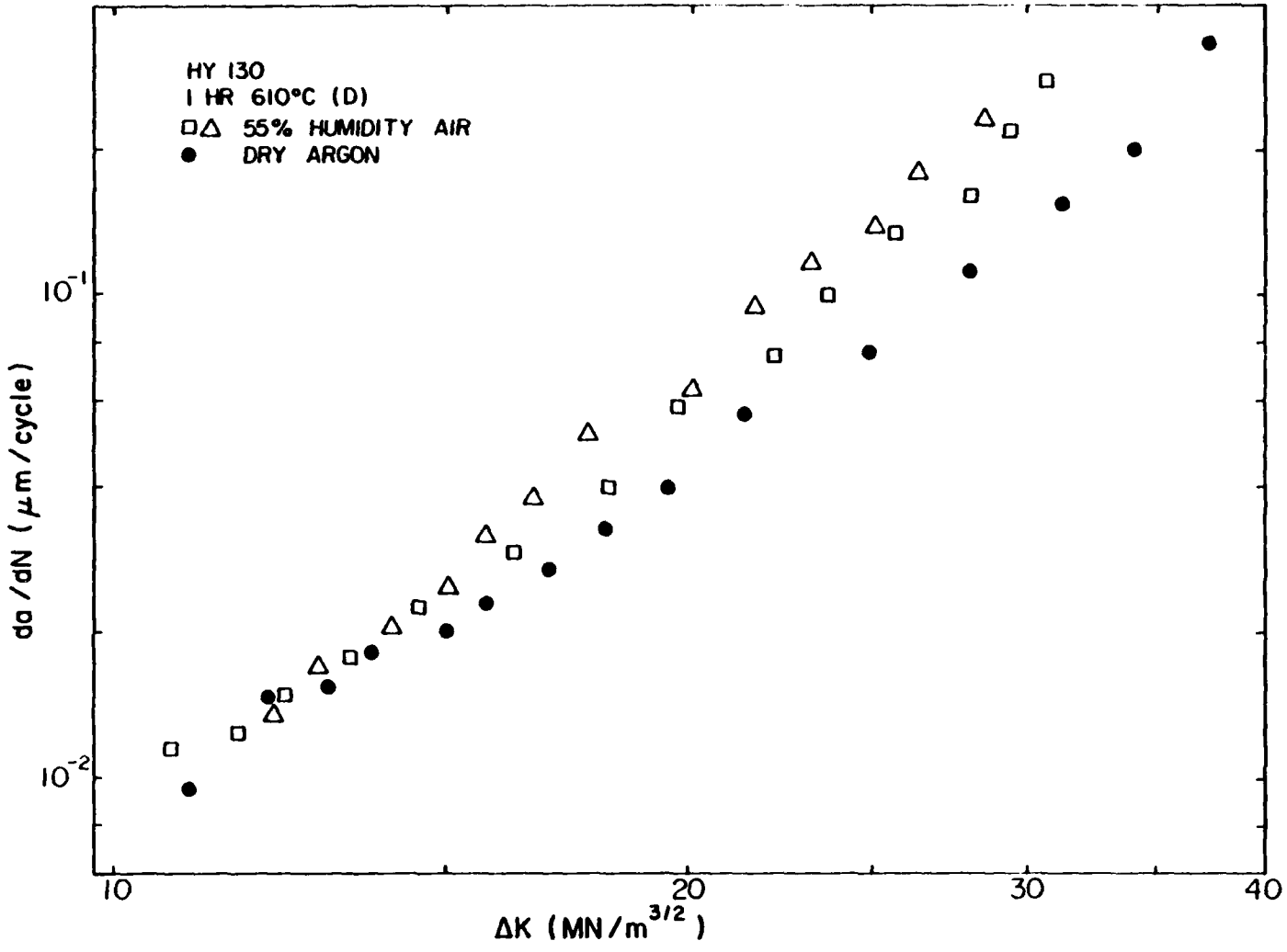

Figure 9. Fatigue crack propagation rate versus ΔK of HY130 austenitized at 815°C and tempered 1 hr at 610°C.

Table 4. Comparison of Fatigue Crack Propagation Rate of HY130 with Different Tempering Treatments

Heat Treatments			C(10^{-12} m^{-1})	m	da/dN* (10^{-8} m/cycle) $\Delta K=15$ MN/$m^{\frac{3}{2}}$	$\Delta K=20$ MN/$m^{\frac{3}{2}}$	$\Delta K=30$ MN/$m^{\frac{3}{2}}$
A	10 hrs, 400° C	Argon	1.09	3.53	1.6	4.3	21
		Air	2.79	3.33	2.5	6.0	24
B	5 hrs, 550° C	Argon	5.34	3.00	1.8	4.3	15
		Air	7.99	2.93	2.3	5.3	16
C	$\frac{1}{4}$ hr, 650° C	Argon	2.17	3.34	1.9	4.8	18
		Air	2.63	3.31	2.1	5.3	20
D	1 hr, 610° C	Argon	8.84	2.86	2.1	4.7	14
		Air	6.47	3.07	2.6	6.4	24

* the standard deviation of the scatter band is less than ± 12.5%

COMPARISON OF NEAR THRESHOLD FATIGUE CRACK PROPAGATION RATE IN HY80 AND HY130, STANDARD HEAT TREATMENT

The first near threshold fatigue crack propagation rate measurements were on HY80 and HY130 with the standard heat treatments and on 4140 tempered at 650° C for comparison. The tests were done in laboratory air of 47% humidity. As previously mentioned, the measurements were made by the load shedding technique in panel specimens 100 mm by 3.5 mm by 25 mm containing a 3 mm by 0.2 mm center notch introduced by spark machining. The load was reduced in steps less than 8% of the previous load. The steps were less than 5% as ΔK_{th} was approached. ΔK_{th} was taken to be the ΔK below which no crack growth was detected in 3×10^6 cycles. After ΔK_{th} was determined, the load was increased and da/dN was measured under constant nominal stress. The results for the three materials are shown in Figs. 10, 11, and 12. The lowest data point plotted is the maximum possible rate, i.e., the maximum crack advance which could not be detected divided by the number of cycles. HY80 has the highest threshold, 4.2 $MN/m^{\frac{3}{2}}$, while 4140-T650 has the lowest, 3.5 $MN/m^{\frac{3}{2}}$.

It is generally considered that the threshold stress intensity range, ΔK_{th}, for macrocrack propagation decreases as the yield stress increases.[17] This probably arises because the material's ductility reduces the local stress at the crack tip more for a low yield stress material than for a high yield stress material (α in Eq.(3)). Thus α and σ_y are inversely related. The present results do not exactly fit the correlation of ΔK_{th} with yield stress, as shown in Table 5. The 4140 steel tempered at 650° C is intermediate in strength between HY80 and HY130 yet it has the lowest ΔK_{th}. For a given yield stress an increase in α with decrease in C content is not unexpected. The difference in ΔK_{th} between HY80 and HY130 was quite

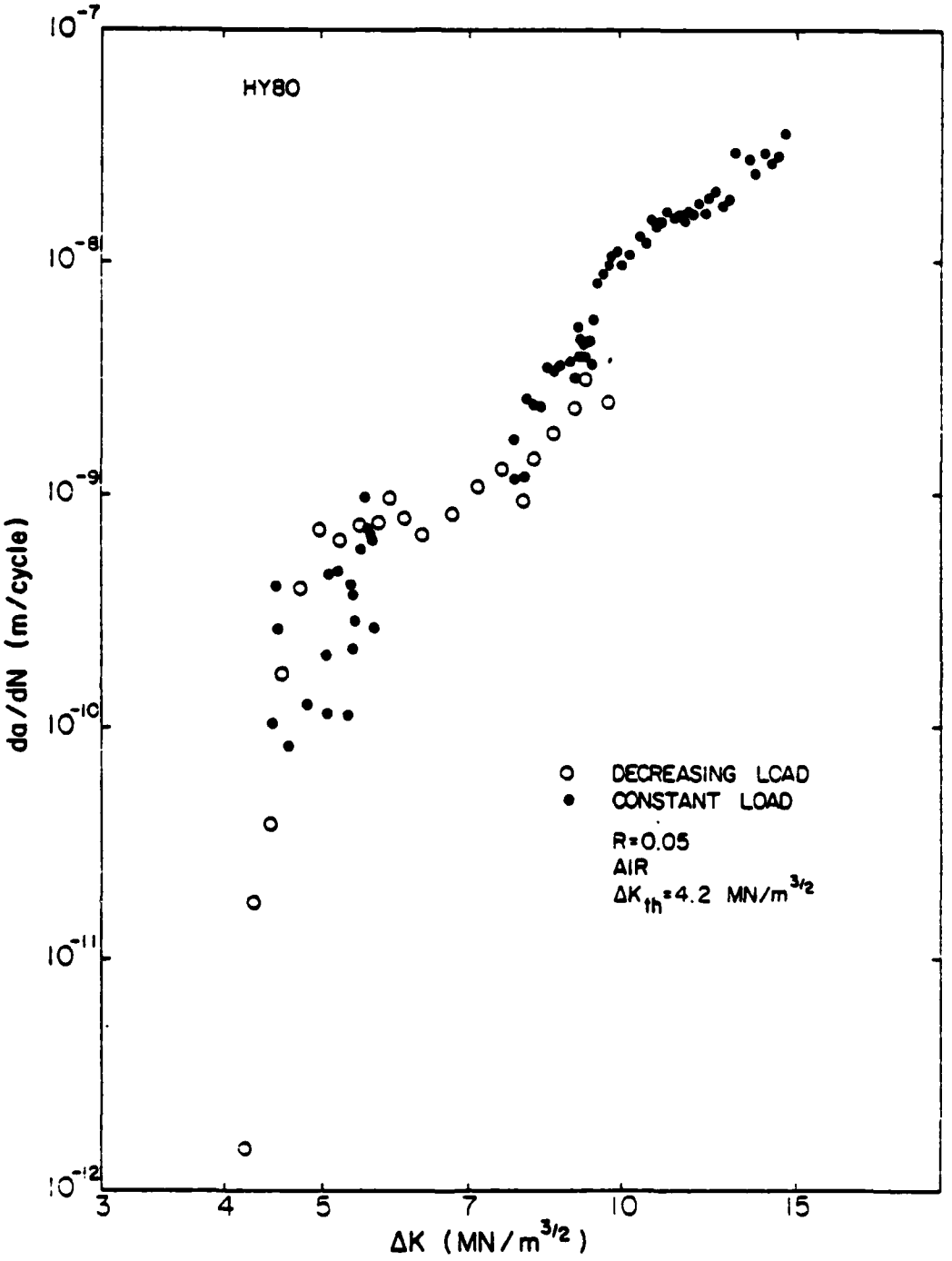

Figure 10. Fatigue crack propagation rate near threshold versus ΔK for HY80 steel.

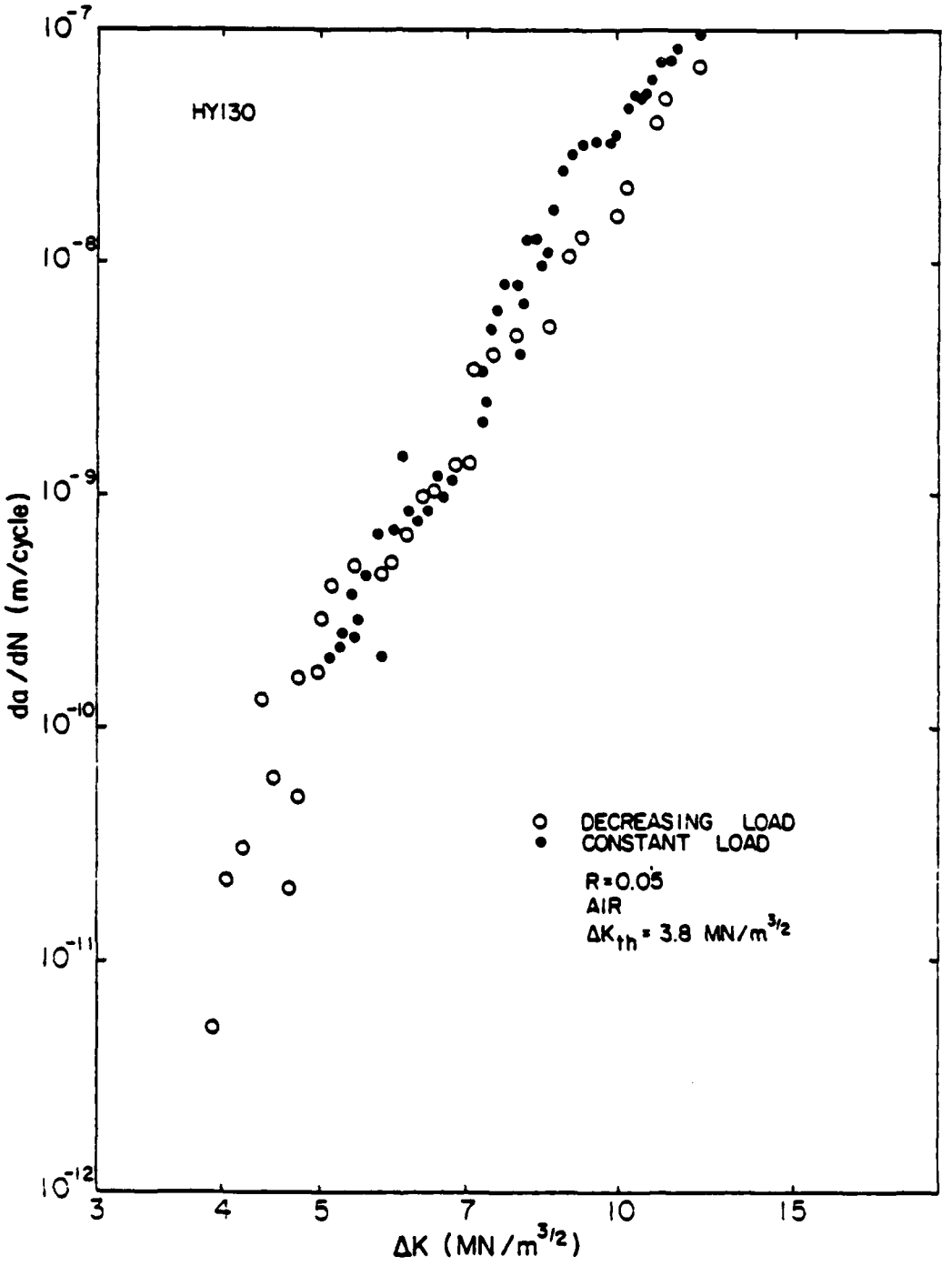

Figure 11. Fatigue crack propagation rate near threshold versus ΔK for HY130 steel.

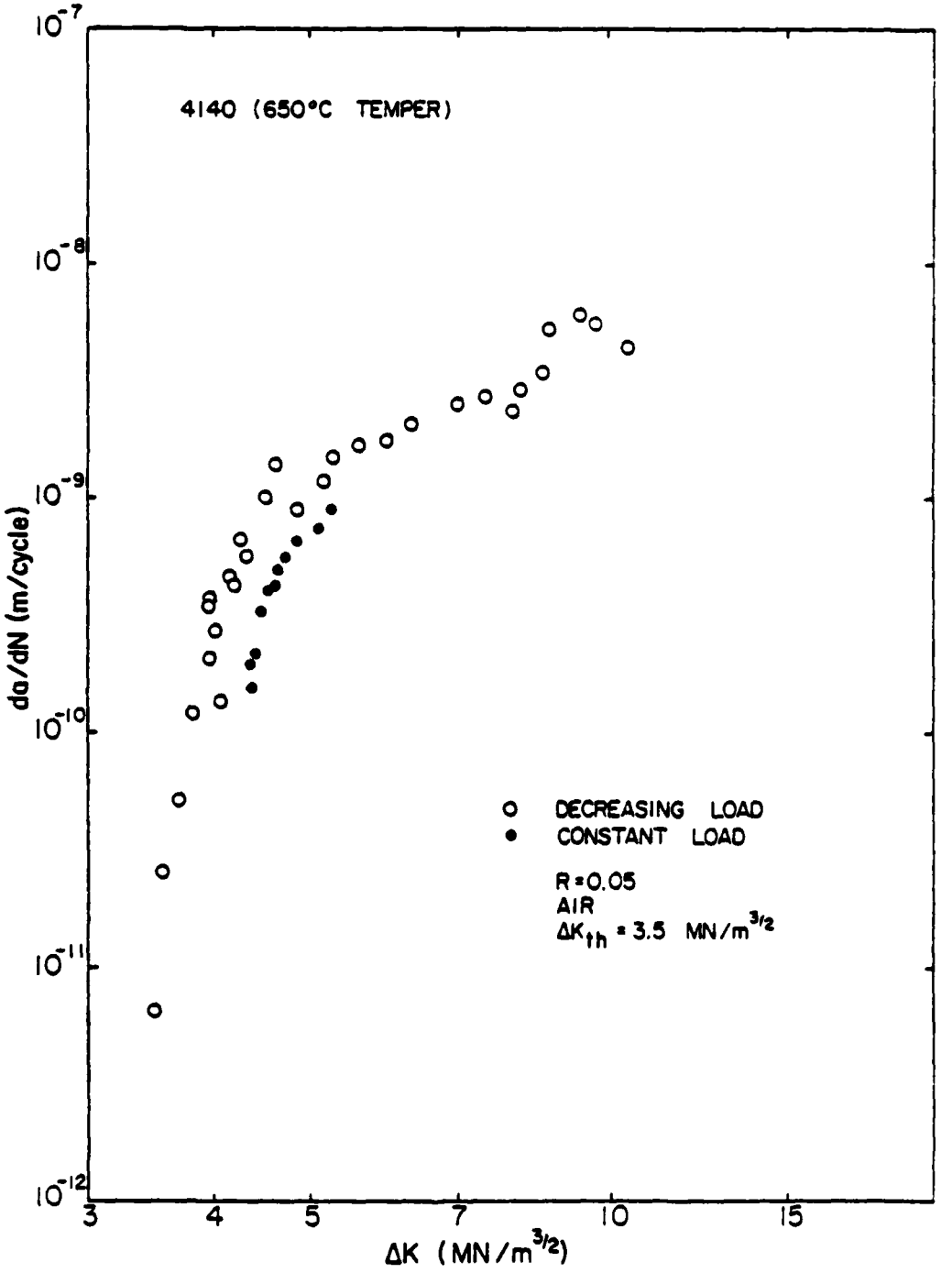

Figure 12. Fatigue crack propagation rate near threshold versus ΔK for 4140 steel tempered 1 hr at 650° C.

Table 5. Yield Strength and ΔK_{th} for HY80, HY130 and 4140 Steels

	$\sigma_y(0.2)$ (monotonic) MN/m^2	$\sigma_y'(0.2)$ (cyclic) MN/m^2	ΔK_{th} $MN/m^{\frac{3}{2}}$
HY80 (700° C)	626	521	4.2
HY130 (610° C)	1042	868	3.8
4140 (650° C)	885	555	3.5

The temperatures, in parentheses, are the tempering temperatures. Environment, air.

small (4.2 vs. 3.8 $MN/m^{\frac{3}{2}}$) even though there are large differences in monotonic yield stress (626 vs. 1042 MN/m^2) and cyclic yield stress (521 vs. 868 MN/m^2). This is proposed to be due to compensating changes in σ_s and α. Also s may be smaller in HY130 because it has a higher dislocation density which is expected to increase the source density.

The microstructure of 4140 steel (650° C temper) after plastic strain cycling consists of a dislocation cell structure with a very low density of dislocations inside the cells plus large globular cementite particles.[18] The low ΔK_{th} in this steel may be associated with the cementite particles because they may be vulnerable sites due to stress concentration. Comparing HY80 and HY130, the lower C content and lower tempering temperature in HY130 means that it is at an earlier stage of tempering, i.e., lower carbide size. Also, addition of V to HY130 results in VC rather than Fe_3C giving much smaller carbide size. Thus, any stress concentration around carbides is expected to play a smaller role in HY130.

EFFECT OF TEMPERING TEMPERATURE ON THRESHOLD STRESS INTENSITY FOR FATIGUE CRACK PROPAGATION IN HY130

As already described in this report, four tempering heat treatments (A-10 hrs, 400° C; B-5 hrs, 550° C; C-1 hr, 610° C and D-$\frac{1}{4}$ hr, 650° C) for HY130 were devised to give the same approximate hardness, 31-33 Rockwell C.

The fatigue crack propagation results at intermediate ΔKs in HY130 with these four heat treatments for air and argon environments were nearly identical meaning U is nearly the same for all. This same series of heat treatments is of interest for a study of ΔK_{th} because fixing hardness should to a first approximation fix σ_s and α in Eq.(3), but the s values are expected to be different and thus a variation in ΔK_{th} might be expected if one believes Eq.(3).

The crack propagation rates near ΔK_{th} in HY130 with the different heat treatments are shown in Figs. 13-16. The intermediate ΔK data from the previous section are plotted in the same figures. The near threshold fatigue crack progagation results are summarized in Table 6. The four sets of data are compared in Fig. 17. The standard treatment, tempering 1 hr at 610° C, gave the lowest da/dN at ΔK of 4 MPa $\sqrt{m}$ and highest ΔK_{th}, 3.6 MPa $\sqrt{m}$.

Scanning electron microscopy was used to examine the fracture surfaces near the threshold region. The scanning electron micrographs of the fatigue fracture surfaces of specimens tempered 1 hr at 610° C and 10 hrs at 400° C are shown in Figs. 18 and 19 respectively. In Fig. 18 the fracture morphology shows a ductile transgranular fracture mode to have occurred. The morphology is similar at intermediate ΔKs. While the fracture mode for 10 hrs at 400° C is also mostly transgranular, Fig. 19, there are some intergranular facets. The proportion of intergranular facets is reduced with increase in ΔK. The lower ΔK_{th} for this treatment may be due to the embrittling intergranular fracture mode resulting in a lower value of α. Note the roughness of the fracture surfaces are approximately the same so one expects no increase in ΔK_{th} from crack closure.

Neglecting the above effects, one may discuss the ΔK_{th} variation in terms of variation in s, the distance between the crack tip and the nearest

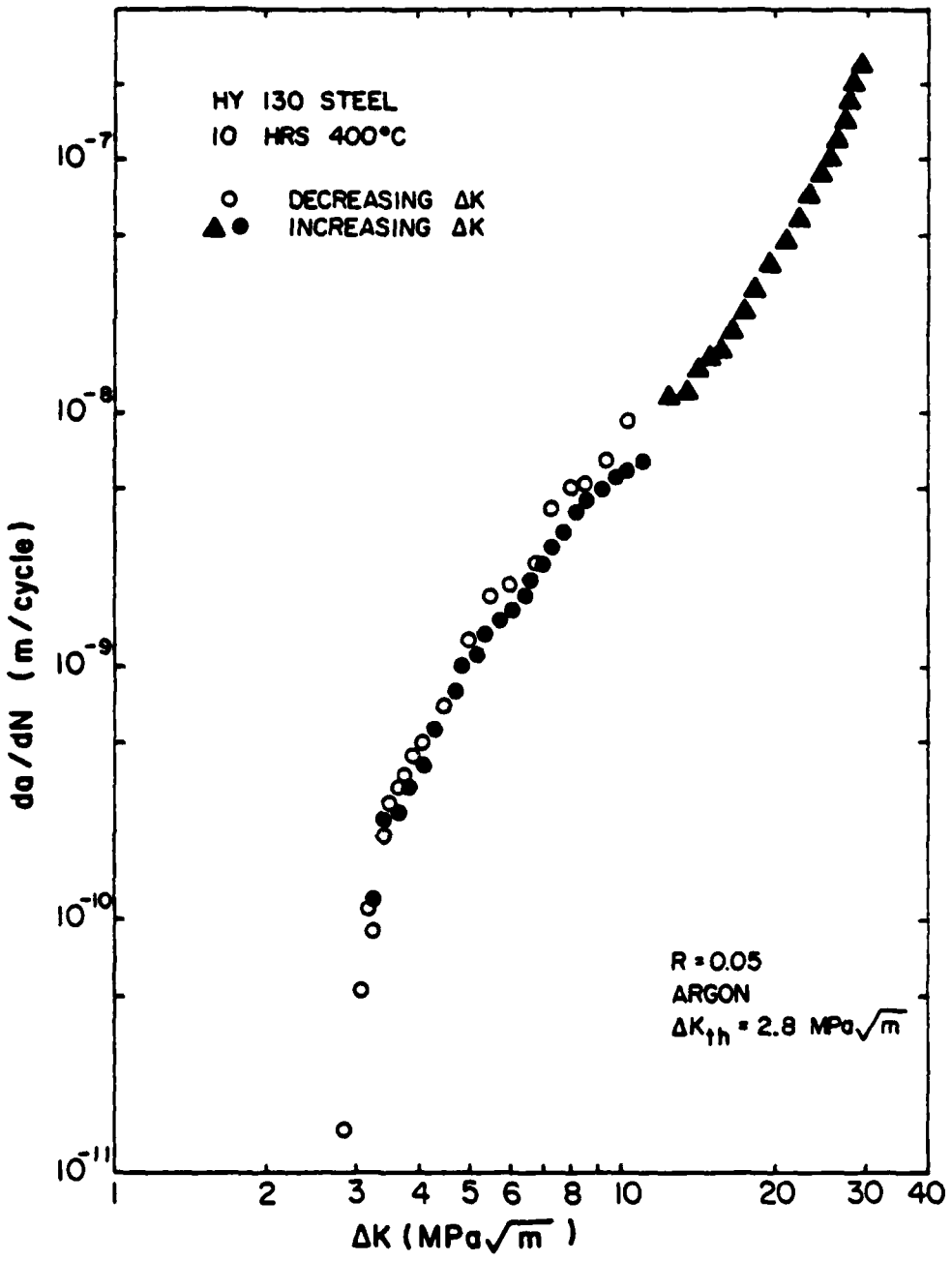

Figure 13. Fatigue crack propagation rate versus ΔK in HY130 steel with tempering at 400° C for 10 hours.

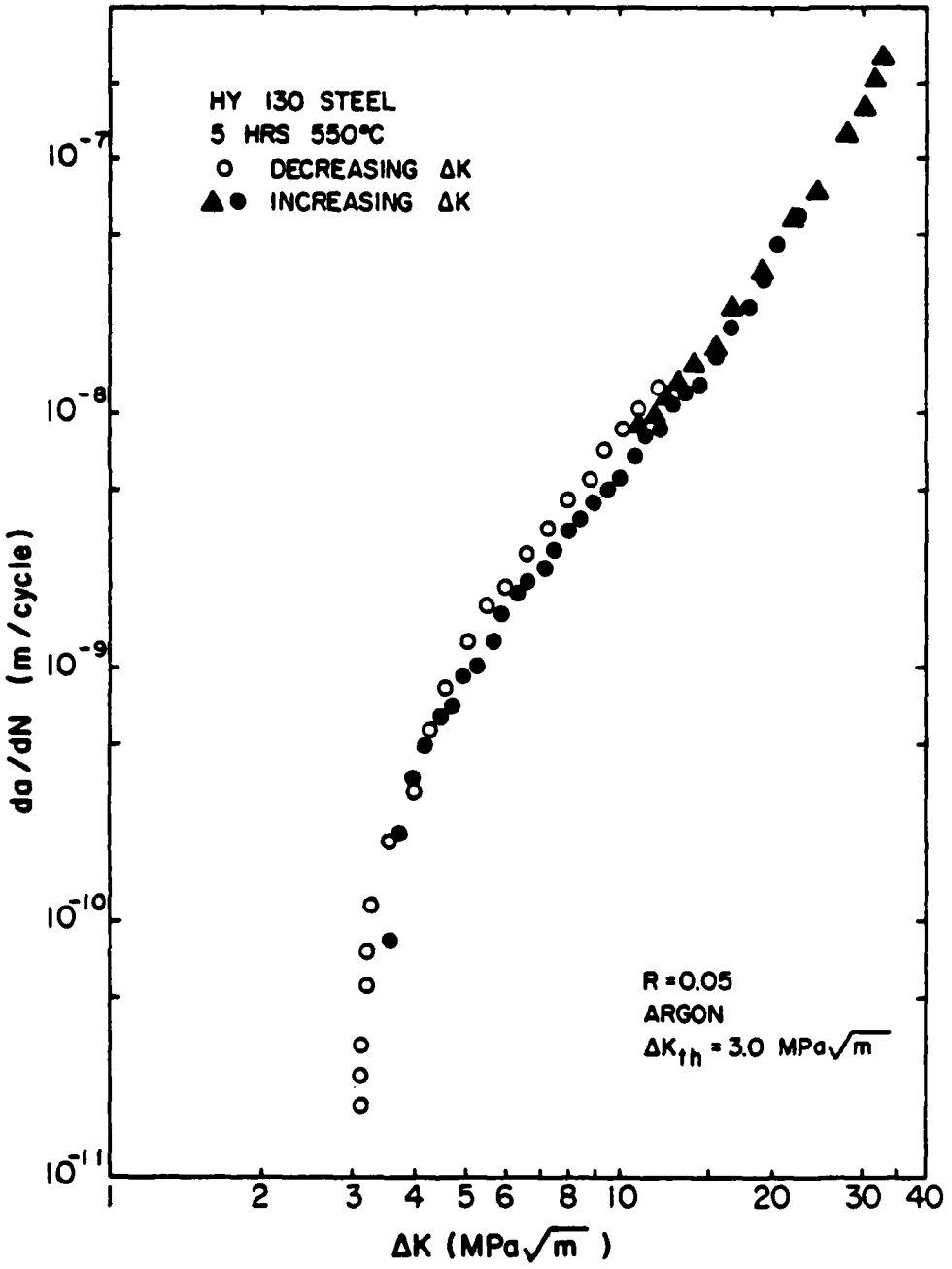

Figure 14. Fatigue crack propagation rate versus ΔK in HY130 steel with tempering at 550° C for 5 hours.

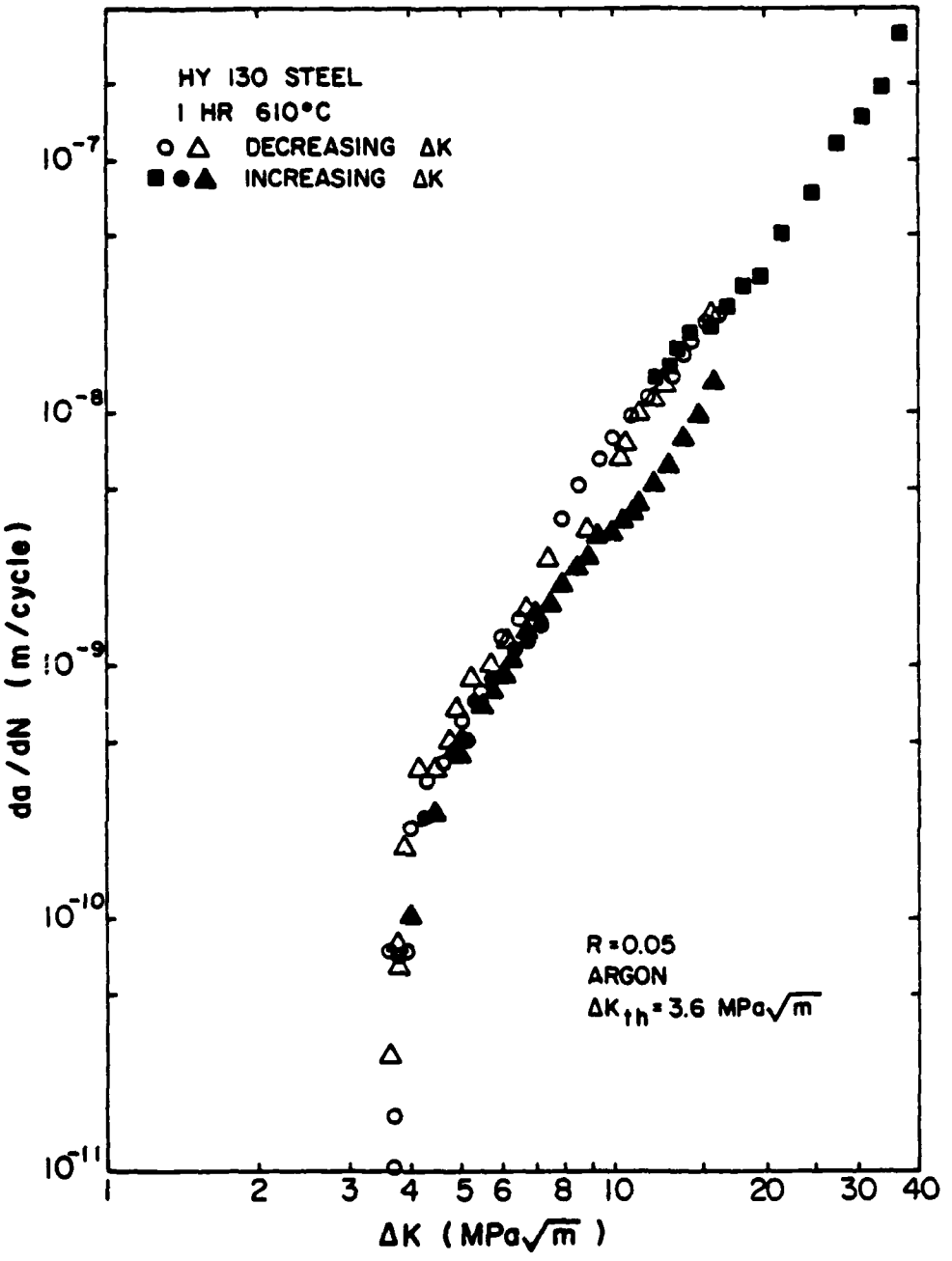

Figure 15. Fatigue crack propagation rate versus ΔK in HY130 steel with tempering at 610°C for 1 hour.

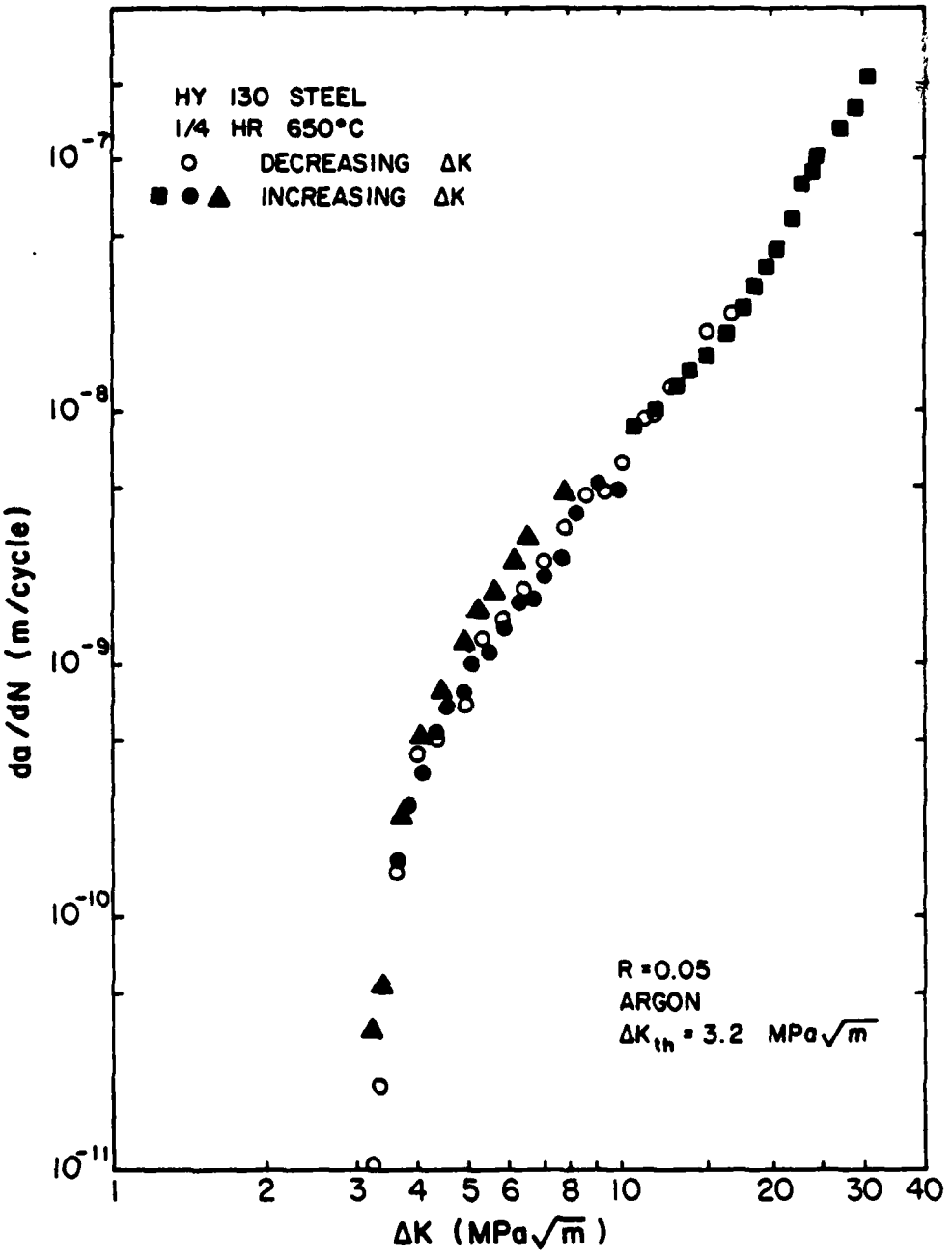

Figure 16. Fatigue crack propagation rate versus ΔK in HY130 steel with tempering at 650°C for $\frac{1}{4}$ hour.

Table 6. Fatigue Crack Propagation Rate Data of HY130 for Four Tempering Treatments

	Heat Treatments	Hardness (R.C. Scale)	ΔK_{th} (MPa $\sqrt{m}$)	da/dN (m/cycle) (at ΔK = 4 MPa $\sqrt{m}$)	da/dN (m/cycle) (at ΔK = 20 MPa $\sqrt{m}$)
A	10 hrs, 400°C	33	2.8	4.5×10^{-9}	4.3×10^{-8}
B	5 hrs, 550°C	33	3.0	4.2×10^{-9}	4.3×10^{-8}
C	1 hr, 610°C	33	3.6	1.5×10^{-9}	4.7×10^{-8}
D	$\frac{1}{4}$ hr, 650°C	31	3.2	3.8×10^{-9}	4.8×10^{-8}

All done in dry argon

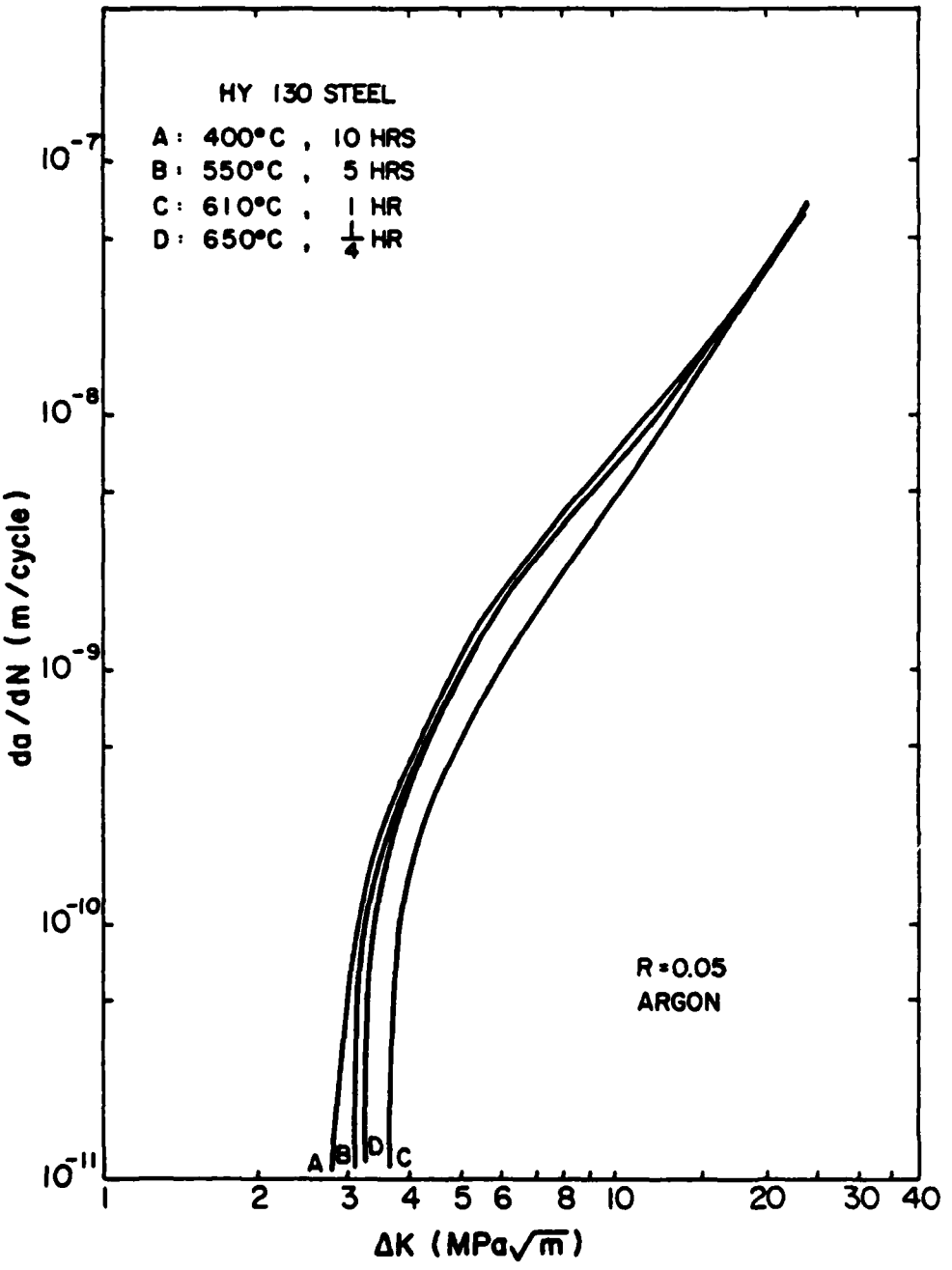

Figure 17. Variation of fatigue crack propagation rate versus ΔK in HY130 steel with various tempering treatments.

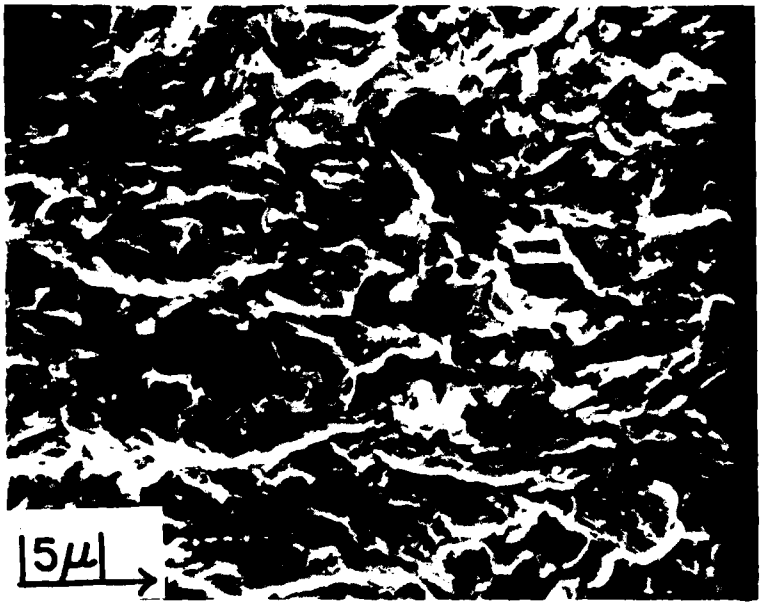

Figure 18. Scanning electron micrograph of the fatigue fracture surfaces of HY130 tempered 1 hr at 610° near threshold region ($\Delta K \sim 4$ MPa$\sqrt{m}$). The arrow shows the direction of crack propagation.

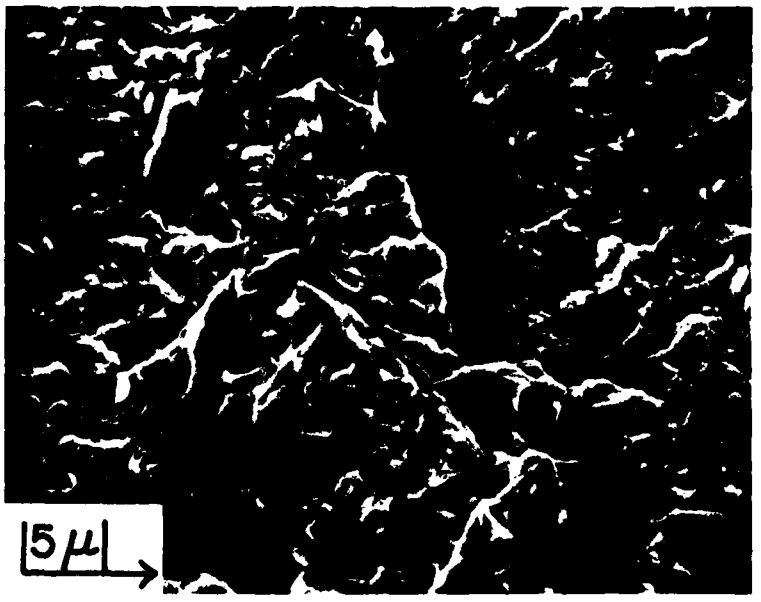

Figure 19. Scanning electron micrograph of the fatigue fracture surfaces of HY130 tempered 10 hrs at 400°C near threshold region ($\Delta K \sim 3$ MPa$\sqrt{m}$). The arrow shows the direction of crack propagation.

dislocation source. If one assumes that dislocation segments pinned between carbide particles acts as dislocation sources, then s and ΔK_{th} are expected to increase with tempering temperature in the constant hardness series. The increase in tempering temperature from 400 to 610°, at constant hardness, does cause an increase in ΔK_{th}; however, the increase from 610 to 650° C causes a decrease. The hardness is also somewhat lower for this treatment. In any respect, the standard heat treatment for HY130 gave the best resistance to near threshold fatigue crack growth of all those tested.

NEAR THRESHOLD FATIGUE CRACK PROPAGATION RATE OF HY80 WITH DUAL PHASE MICROSTRUCTURE

Dual phase structured steels containing comparable amounts of martensite and ferrite have recently been shown to have a very good combination of strength and ductility when compared with traditionally heat-treated steels. For example, in a Ni-Cr-Mo-V steel Woodford[19] showed that the proper dual phase heat treatment dramatically reduced the transition temperature and temper embrittlement. McEvily and co-workers[9] have shown that certain dual phase structures give much higher ΔK_{th} for fatigue crack propagation in 1018 steel when compared to conventional heat treatment. The stress intensity threshold range, ΔK_{th}, is a function of microstructure such that generally in the same material lower strength is accompanied by a higher ΔK_{th} value. However, McEvily and co-workers observed that ΔK_{th} in 1018 steel for a dual phase microstructure where martensite is the continuous phase is much higher than for the normalized condition even though the strength of the latter steel is higher. The origin of this effect was not known. Thus the effect of dual phase microstructures on threshold stress intensity for fatigue crack propagation, ΔK_{th}, is an important subject for study from a theoretical as well as practical basis and HY80 steel is a good candidate

for such a study.

The threshold stress intensity fatigue testing was done in dry argon using the procedures given in the previous section. The closure stress was measured by the foil strain gage method.[20] Two foil strain gages (Micro-Measurements MA-06-008CL-120) were cemented on each center notch specimen near the expected crack path at different distances from the notch tip. From the deviation from linearity in the stress-local strain curve the closure stress was determined.

Two different dual phase microstructures were developed in HY80. Table 7 shows the heat treatment procedures compared to the standard quenched-tempered heat treatment. The hardness resulting from each treatment is also given.

Table 7. Heat Treatment of HY80 to Produce Dual Phase Microstructures

		Hardness (R_c)
Dual Phase IAA	1000°C, 3 hrs → furnace cool → 750° C, 2 days → water quench	38
Dual Phase IAB	1000° C, 3 hrs → furnace cool → 900° C, 1 hr → water quench → 700° C, 1 hr → water quench → 750° C, 2 days → water quench	35
Standard Heat Treatment	1000° C, 3 hrs → furnace cool → 900° C, 1 hr → water quench → 700° C, 1 hr → water quench	20

The dual phase microstructures resulting from heat treatments IAA and IAB steels are shown in Fig. 20(a) and Fig. 20(b) respectively. As determined by SEM microprobe, the bright phase which contains larger amounts of Ni, Mo and Cr is martensite and the dark phase is ferrite. From TEM thin foil observation (Figs. 20(c and d)), the martensite width is 0.2-1.0 μm in IAB dual phase and 0.5-2.0 μm in IAA with most of martensite regions being interconnected. The austenite phase formation in IAB steel during inter-

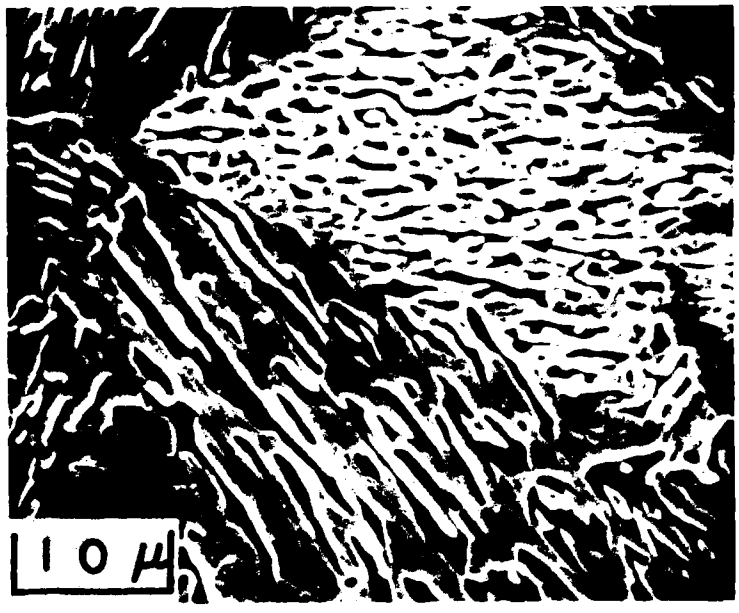

(a)

(b)

Figure 20. Electron micrographs of HY80 dual phase steel.
(a) SEM of the dual phase IAA
(b) SEM of the dual phase IAB

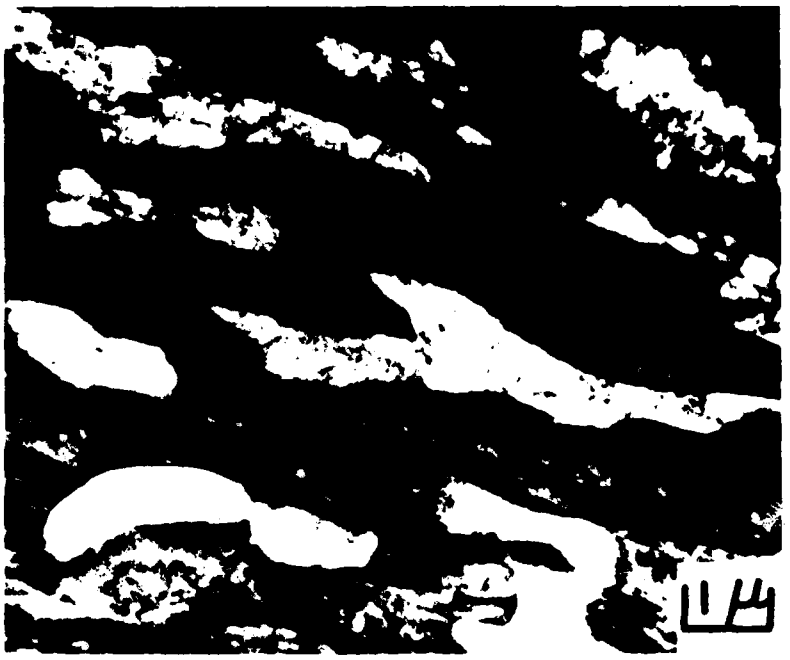

(c)

(d)

Figure 20. (c) TEM of the dual phase IAA
(d) TEM of the dual phase IAB

critical annealing seems to be not as complete as IAA steel. The IAA microstructure contains interconnected martensite regions inside the prior austenite grains. Such was not observed in IAB. The prior austenite grain size of IAA is about 35 μm and about 12 μm for IAB.

The near-threshold fatigue crack propagation rates are plotted versus ΔK in Figs. 21, 22 and 23. Comparison among them is shown in Fig. 24. The dual phase heat treatment much reduces the fatigue crack propagation rate in the low ΔK region. Compared with the standard heat treatment where ΔK_{th} = 3.1 MPa $\sqrt{m}$, the ΔK_{th} is raised by 40% in the IAB dual phase steel (ΔK_{th} = 4.3 MPa $\sqrt{m}$) and 75% in the IAA dual phase steel (ΔK_{th} = 5.4 MPa $\sqrt{m}$). At higher ΔK, the difference among the propagation rates become smaller. Additionally, the dual phase IAA structure was tempered at 650° C for one hour to achieve the same strength level as the standard heat treatment. Figure 25 shows the results of the fatigue crack propagation rate test. The threshold value (4.4 MPa $\sqrt{m}$) is 42% higher than that resulting from the standard heat treatment.

Several researchers[21,9] have found a fracture mode transition as the near threshold region is approached on lowering ΔK whereby the fracture mode changes from a tensile to a shear mode. The fatigue fracture surfaces were observed by SEM to study this phenomena. Fatigue fracture surfaces of the standard heat treatment are shown in Figs. 26(a) and (b). Near threshold (ΔK = 3.2 MPa $\sqrt{m}$) small shear ridges are distributed on the fracture surface which in general has a ductile appearance and is transgranular. Some small particles are visible no doubt arising from a fretting mechanism. At higher ΔK, 6 MPa $\sqrt{m}$ a typical tensile fracture surface is observed. The roughness level and fracture features in Fig. 26(a) are smaller than those of Fig. 26(b). The fracture surfaces of a dual phase IAB structure specimen

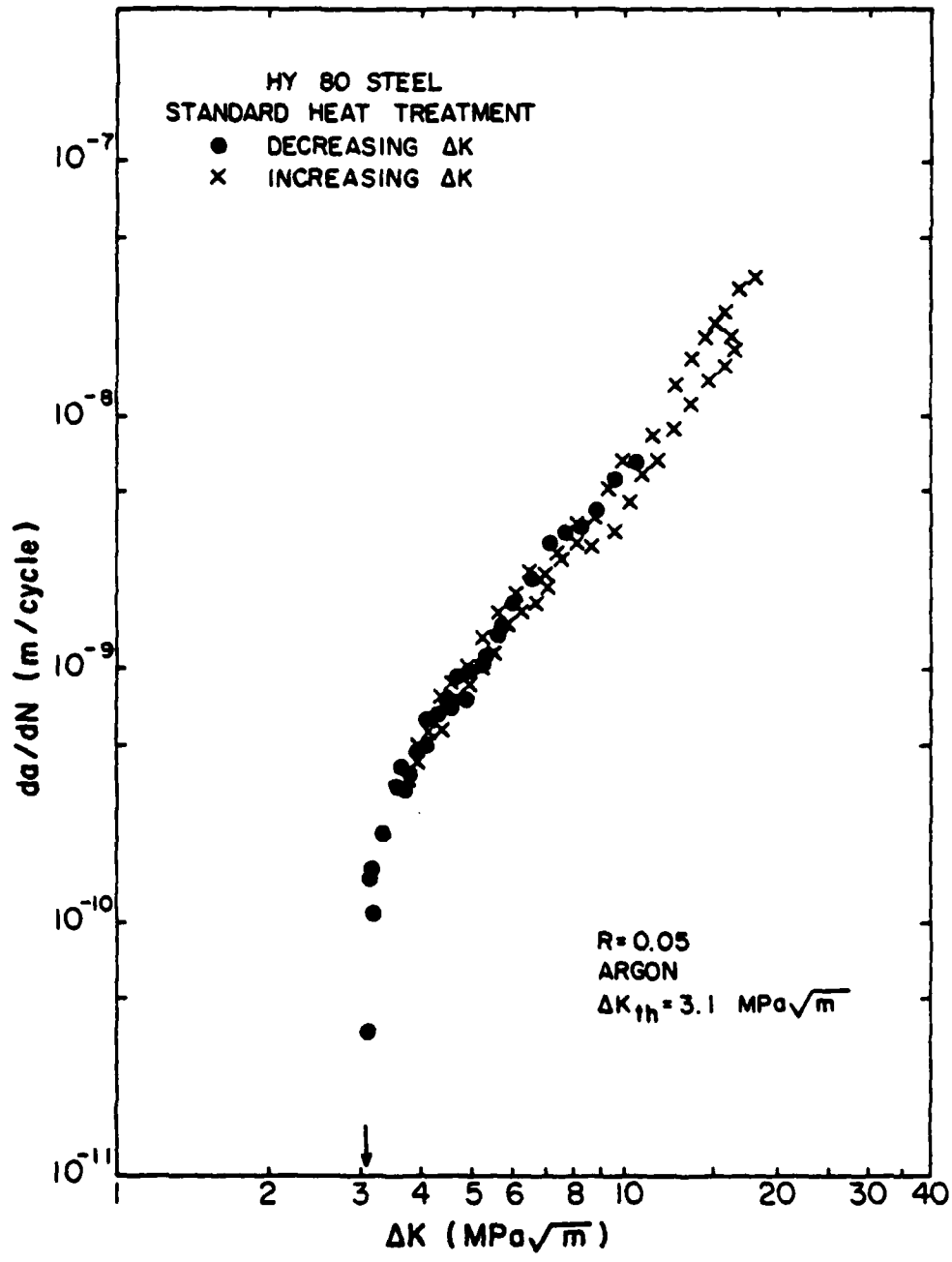

Figure 21. Fatigue crack propagation rate near threshold versus ΔK of the standard heat treatment in HY80 steel.

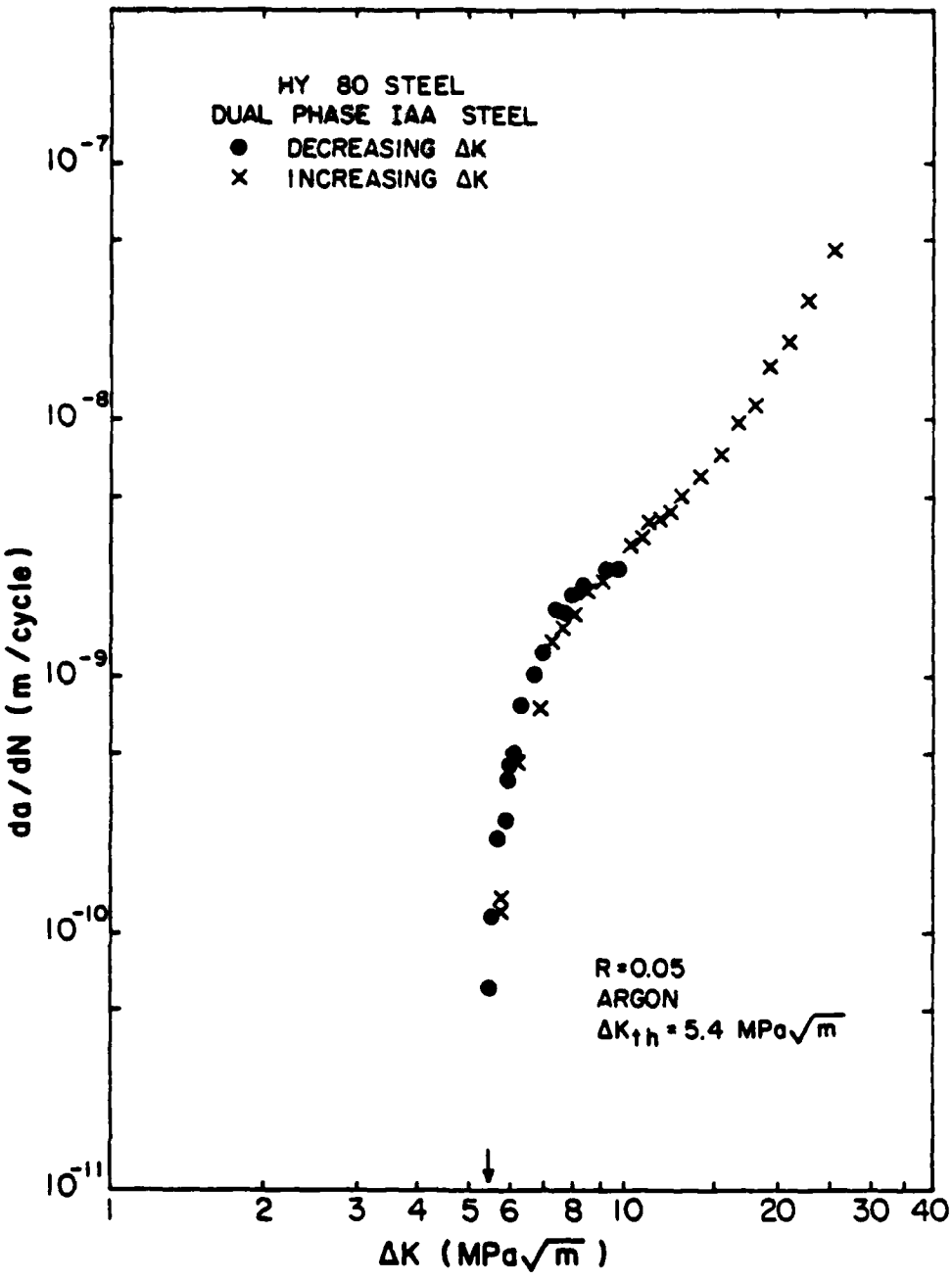

Figure 22. Fatigue crack propagation rate near threshold versus ΔK of the dual phase IAA in HY80 steel.

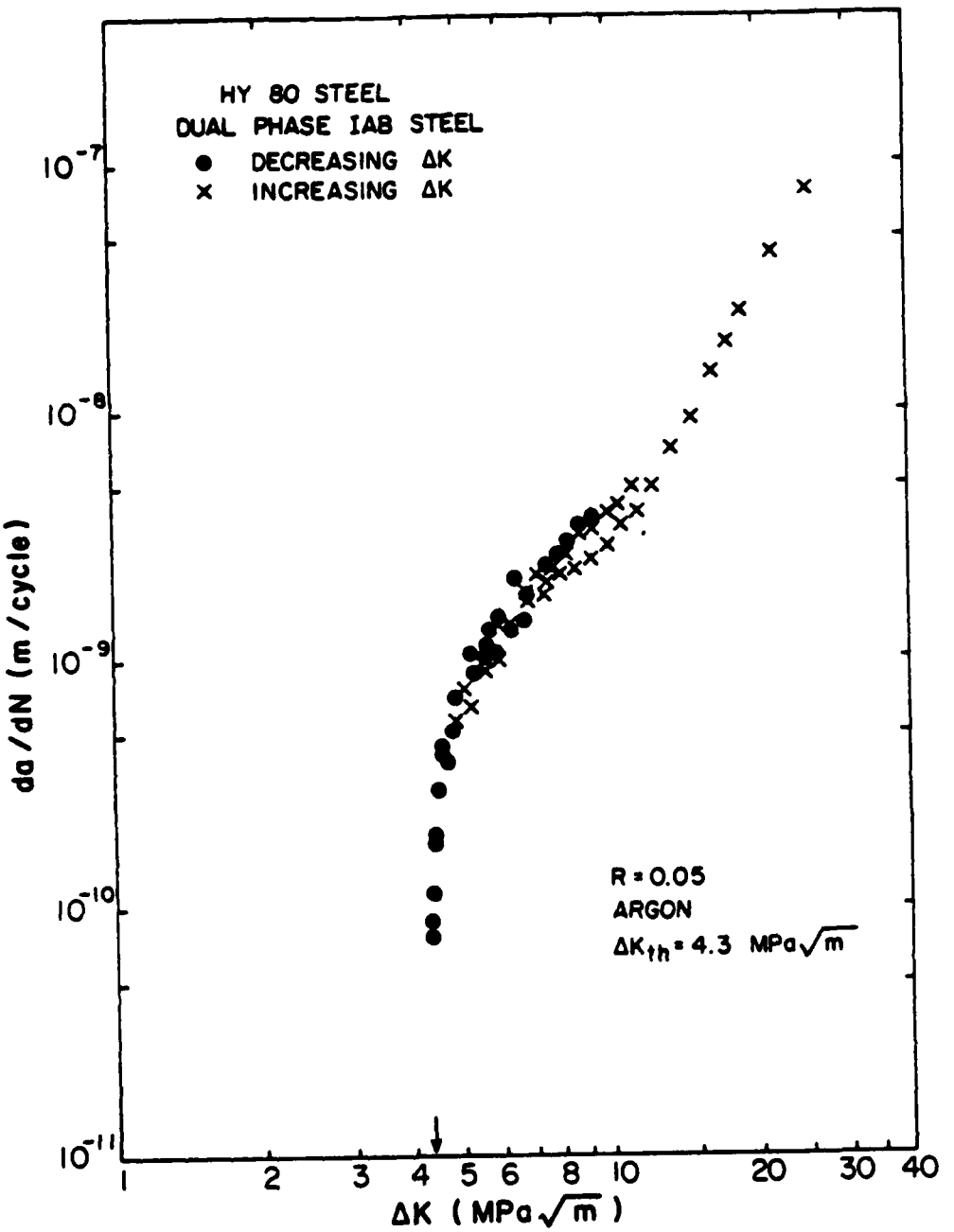

Figure 23. Fatigue crack propagation rate near threshold versus ΔK of the dual phase IAB in HY80 steel.

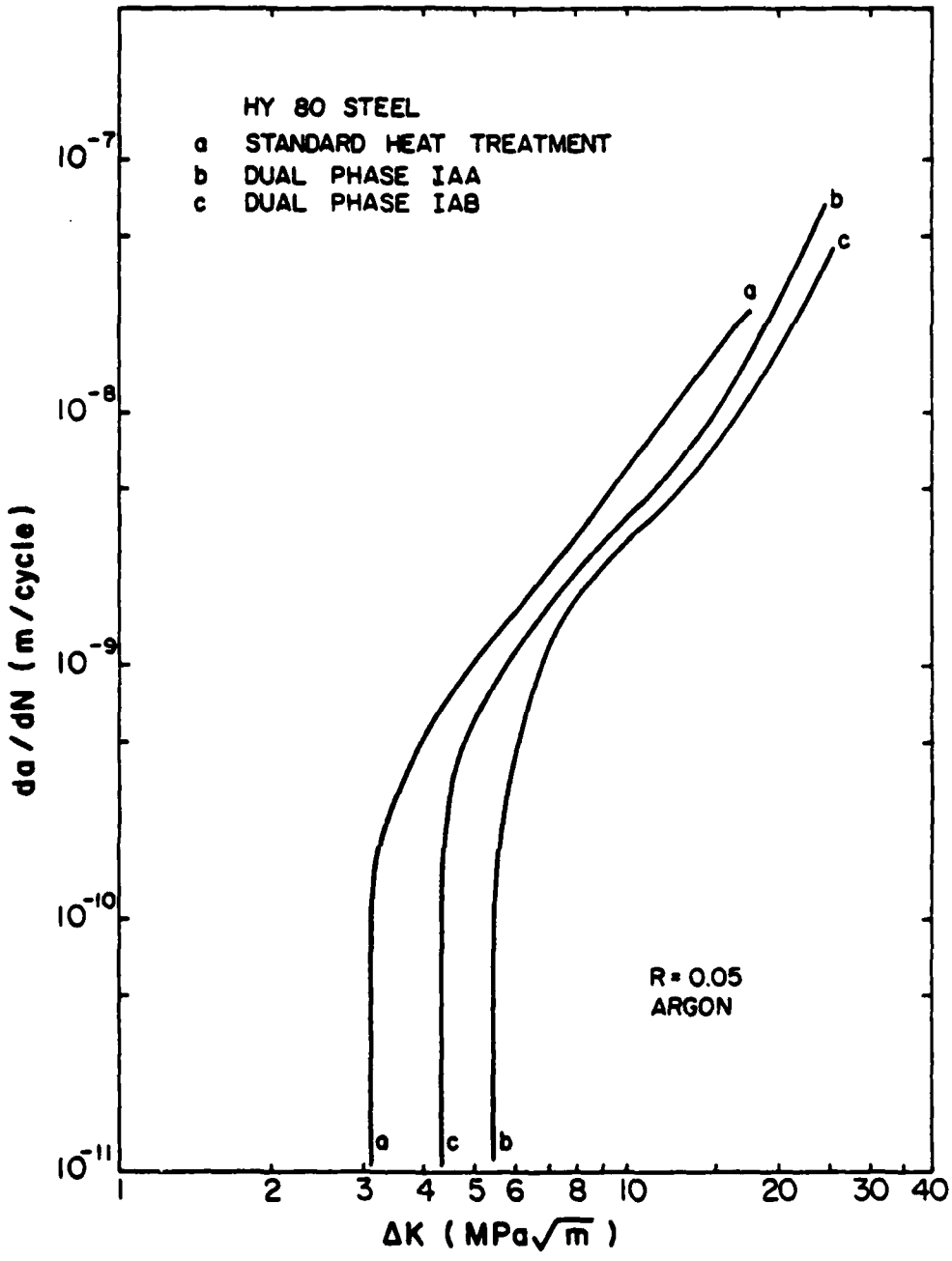

Figure 24. Comparison of fatigue crack propagation rate versus ΔK of various heat treatments in HY80 steel.

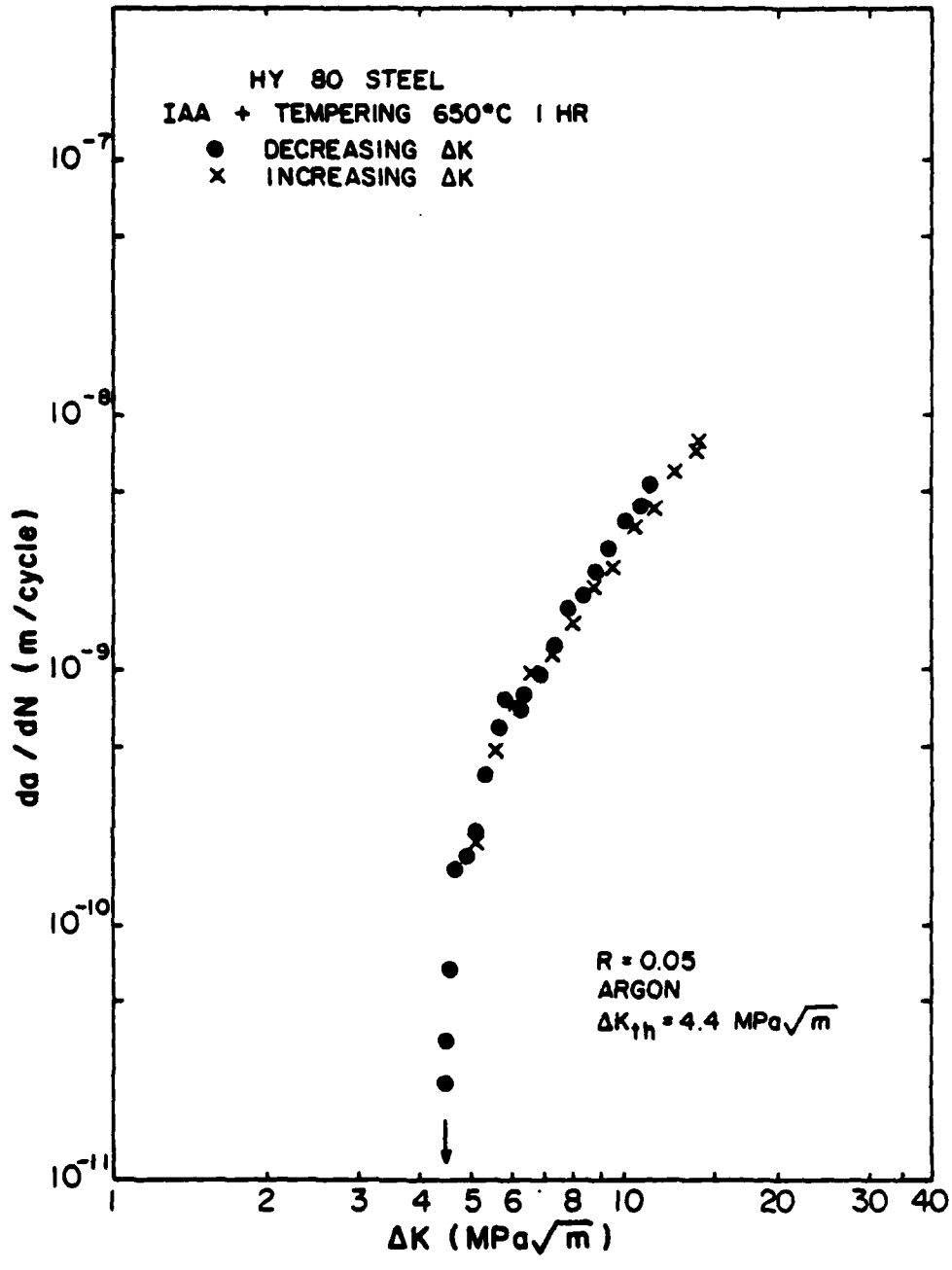

Figure 25. Fatigue crack propagation rate near threshold versus ΔK of the dual phase IAA followed by tempering at 650°C 1 hour in HY80 steel.

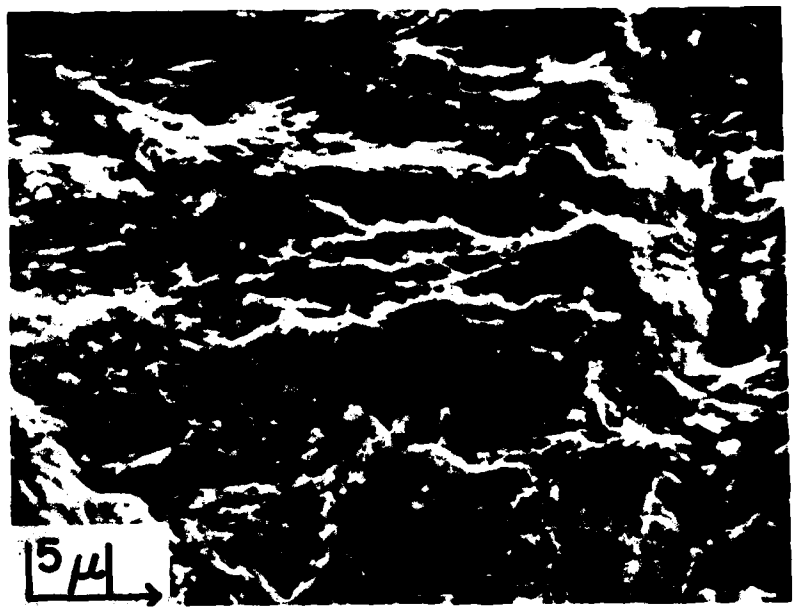

(a)

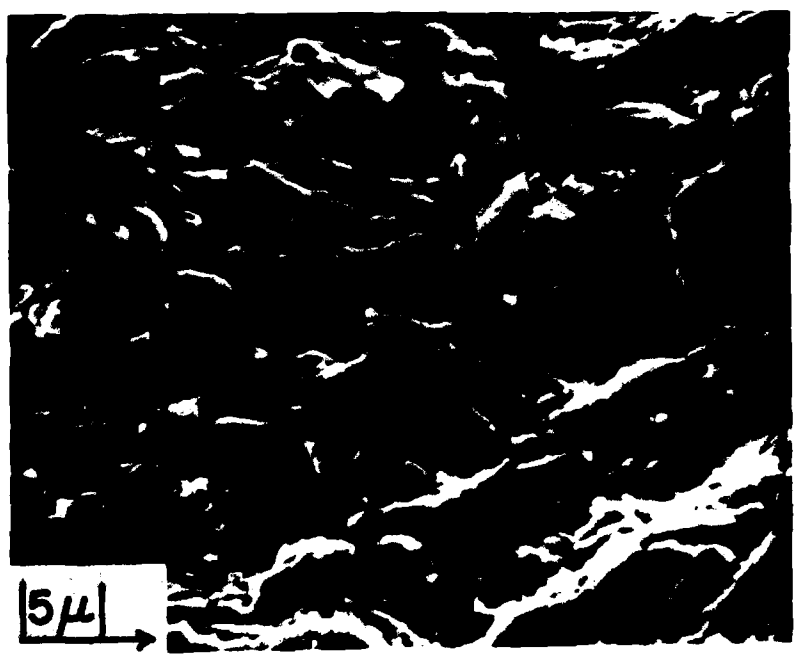

(b)

Figure 26. Scanning electron micrographs of the fatigue fracture surfaces of the standard heat treatment of HY80 steel.

(a) $\Delta K = 3.2$ MPa$\sqrt{m}$

(b) $\Delta K = 6.0$ MPa$\sqrt{m}$

are shown in Figs. 27(a) and (b). Near threshold a few somewhat larger shear surfaces are seen. The rest of Fig. 27(a) shows a ductile tensile fracture mode. The fracture surface structure in Fig. 27(b) for ΔK of 10 MPa $\sqrt{m}$ additionally shows some secondary cracks and is generally rougher than near ΔK_{th}. The fracture surface resulting from the dual phase IAA heat treatment is shown in Figs. 28(a) and (b). The structure is similar to that resulting from the IAB heat treatment. For IAA, near ΔK_{th} Fig. 28(a) the fracture surface is a rougher surface and contains more shear ridges than the fracture surface for IAB. The shear ridges are parallel within the prior austenite grains. Since the widths of the tempered martensite laths from the standard heat treatment and from the dual phase IAA and IAB heat treatments are very small, most of them less than 1 μm, large shear fracture mode regions as occurs inside large grains of iron near threshold is not generally observed. Figure 27(a) is an exception. However, small shear ridges did occur more or less for all three HY80 structures, the orientation presumably depending on the orientation of the longest dimensions of the microstructure. The higher ΔK_{th} for IAA correlates with a higher density of the shear ridges and a rougher fracture surface. The roughness was quantitatively measured using a profilometer. These data will be discussed later.

The closure stresses were measured to further elucidate the near-threshold fatigue crack propagation behavior. The relationships of the closure stress intensity (K_{cl}) versus ΔK and K_{cl} versus ΔK_{eff} ($\equiv K_{max} - K_{cl}$) are shown in Fig. 29(a) and Fig. 30(a) respectively. It is found that the closure stress intensity is basically constant for the higher ΔK region but the value increases when ΔK_{th} is approached. The dual phase IAA with the highest threshold value also has the highest closure stress

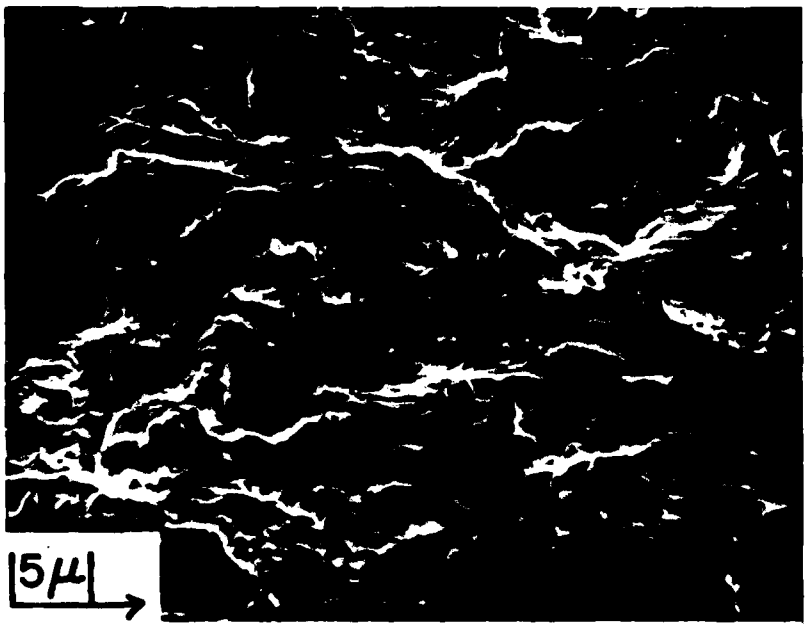

(a)

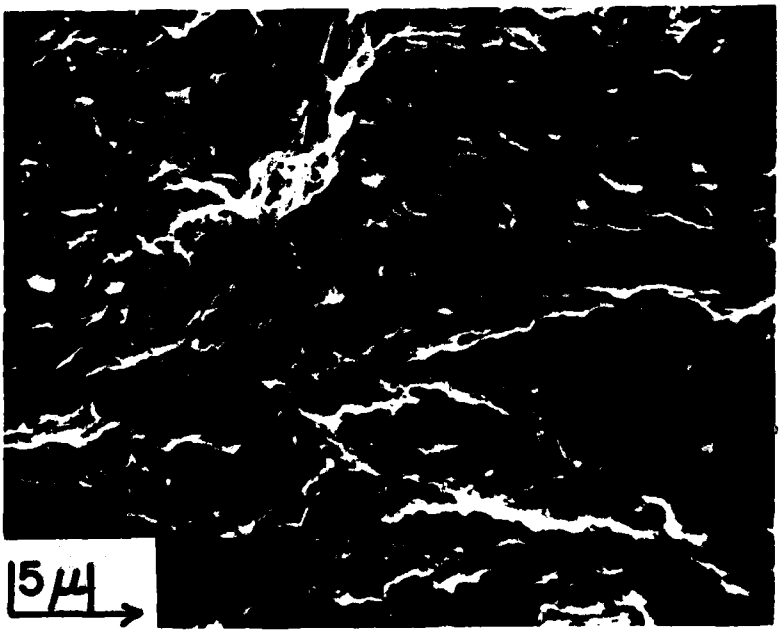

(b)

Figure 27. Scanning electron micrographs of the fatigue fracture surfaces of the dual phase IAB of HY80 steel.

(a) $\Delta K = 4.4$ MPa$\sqrt{m}$

(b) $\Delta K = 10$ MPa$\sqrt{m}$

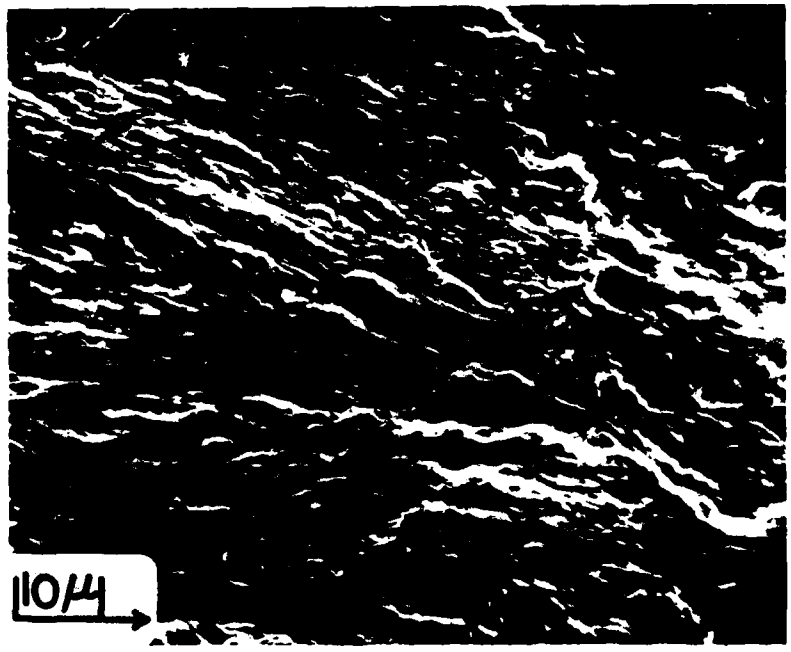

(a)

(b)

Figure 28. Scanning electron micrograph of the fatigue fracture surfaces of the dual phase IAA of HY80 steel.

(a) $\Delta K = 5.6$ MPa$\sqrt{m}$

(b) $\Delta K = 10$ MPa$\sqrt{m}$

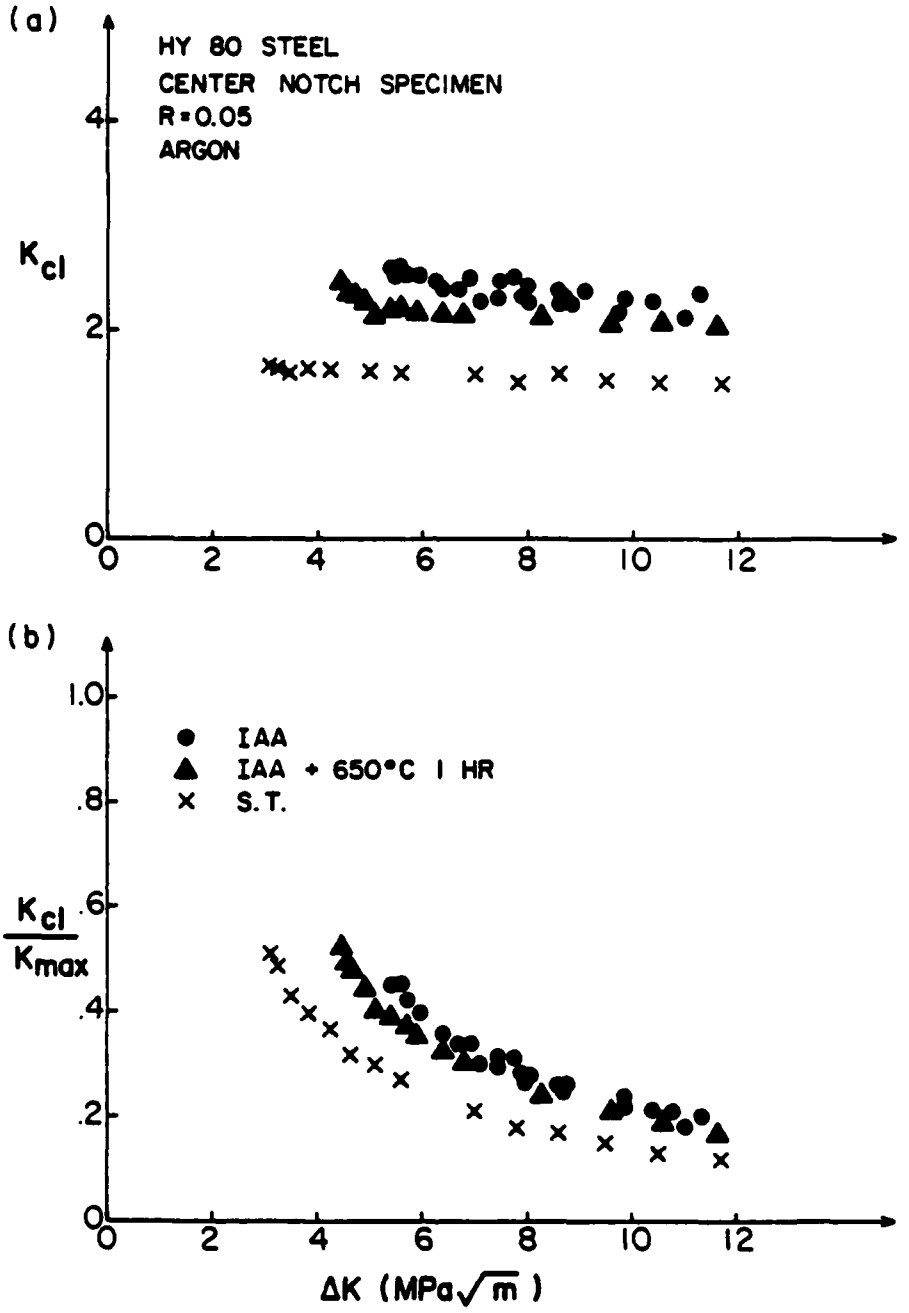

Figure 29. The crack closure behavior of HY80 steel.

(a) Crack closure stress intensity K_{cl} versus ΔK

(b) K_{cl}/K_{max} versus ΔK

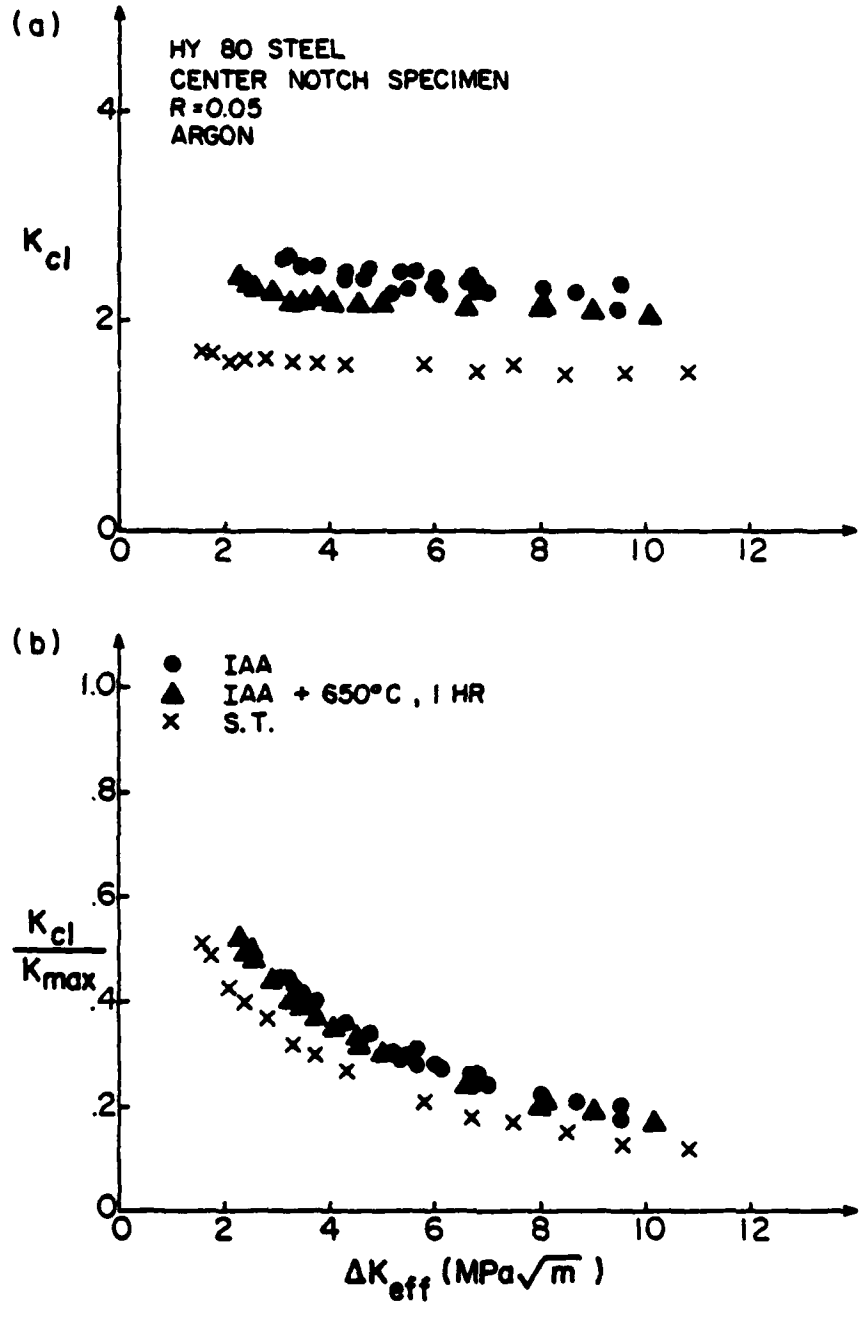

Figure 30. The crack closure behavior of HY80 steel.

(a) Crack closure stress intensity K_{cl} versus ΔK_{eff}

(b) K_{cl}/K_{max} versus ΔK

intensity. When K_{cl} is normalized by K_{max}, Fig. 29(b) and Fig. 30(b), the importance of the closure effect in the near threshold region becomes very obvious. The closure stress intensity near threshold is about 45 to 50% of K_{max} while it is 10 to 20% at ΔK of 12 MPa $\sqrt{m}$. Tempering after the dual phase IAA treatment reduced ΔK_{th}, but ΔK_{th} and the closure stress intensity were still higher than for the standard heat treatment. Figure 31 shows the fatigue crack propagation rates versus ΔK and ΔK_{eff}. In each structure, the convergence between ΔK and ΔK_{eff} curves shows again the crack closure effect is not significant in the intermediate ΔK regime. At low ΔK the difference among ΔK_{eff} of the three structures is smaller than the difference among the ΔK curves. However, the ΔK_{eff} curves do not converge to one curve. Table 8 summarizes some of the results.

Table 8. The Closure Measurements of HY80 Steel

	Hardness (R_c)	ΔK_{th} ($MN/m^{\frac{3}{2}}$)	$K_{cl,th}$ ($MN/m^{\frac{3}{2}}$)	$\Delta K_{eff,th}$ ($MN/m^{\frac{3}{2}}$)	Prior Austenite Grain Size (μm)
Dual Phase IAA	38	5.4	2.5	3.2	35
Dual Phase IAB	35	4.3	-	-	12
Standard Heat Treatment	20	3.1	1.7	1.7	12
IAA + 650°C 1 hr	20	4.4	2.4	2.2	35

The surface roughness of the dual phase IAA and the standard heat treatment was measured in the thickness direction by a profilometer with up to 2000 times magnification. The magnitude of the surface roughness is based on the standard deviation of the recorded surface profile. Comparing crack tip opening displacement (CTOD) at given values of ΔK_s, the results are shown in Table 9.

Figure 32(a) shows the results of surface roughness versus ΔK. The surface roughness monotonically increases as ΔK is increased. Near threshold the roughness of the dual phase IAA is higher than for the standard heat

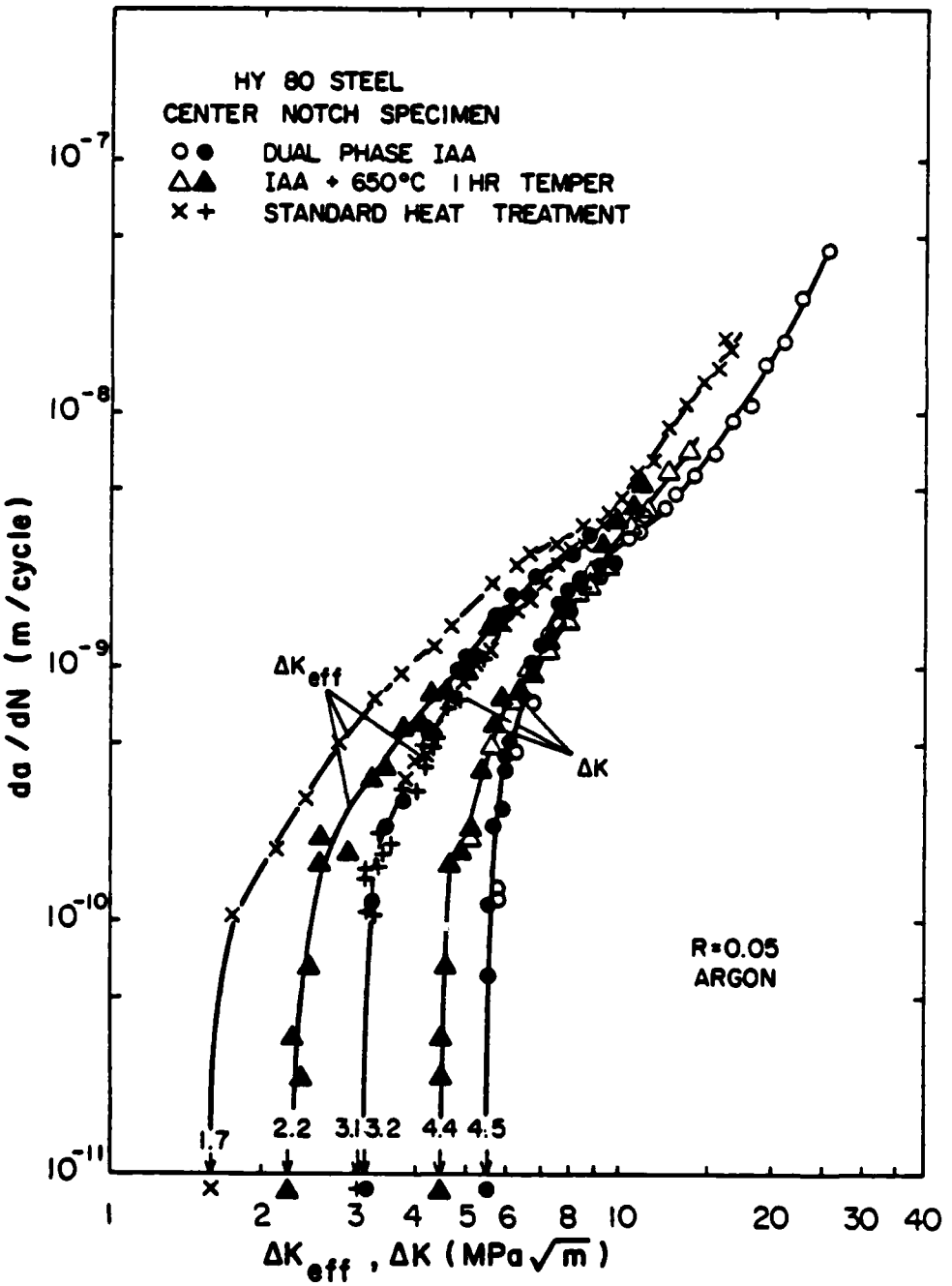

Figure 31. Fatigue crack propagation rate near threshold versus ΔK and ΔK_{eff} in HY80 steel with various heat treatments.

Table 9. Surface Roughness of HY80 Steel

	ΔK ($MN/m^{\frac{3}{2}}$)	$CTOD^*_{max}$ (μm)	Surface Roughness (μm)	Surface Roughness / CTOD
Dual Phase IAA	10	0.32	8.5	27
(σ_y = 829 MN/m^2)	5.6	0.10	4.4	44
Standard Heat Treatment	8.5	0.30	7.4	25
(σ_y = 650 MN/m^2)	6.0	0.15	5.3	36
	3.3	0.045	3.2	72

* $CTOD_{max} = 0.49\ (K_{max}^2/\sigma_y E)$, where E is Young's modulus (= 204 GPa)

treatment. All these are consistent with the SEM observations. Since the roughness level of the fatigue surface is modulated by the crack opening displacement at some specific value of ΔK, the measured surface roughness divided by CTOD at a given value of ΔK can then be regarded as "true" relative surface roughness. Based on this concept, the "true" roughness versus ΔK is shown in Fig. 32(b). In contrast to the surface roughness versus ΔK in Fig. 31(a), the "true" surface roughness indeed increases as ΔK is decreased to the threshold. Near threshold the higher closure level seems to be connected with the higher level of the "true" surface roughness. At the same ΔK, the "true" roughness of IAA is always higher than for the standard heat treatment.

THE TRANSITION BEHAVIOR OF HY130 and HY80 STEELS

In HY130 as already described, four quenched and tempered microstructures were developed with similar strength levels. Yoder et al.[22] proposed that the transition in slope in the log da/dN versus log ΔK curve which occurs between the mid-ΔK and near threshold regions occurs when the cyclic plastic zone size at the crack tip approaches an effective grain size ($\bar{\ell}$). They proposed the following equation for the transition stress intensity: $\Delta K_T = 5.5\ \sigma_y (\bar{\ell})^{\frac{1}{2}}$. The value of $\bar{\ell}$ for HY130 with the different quenched and tempered structures

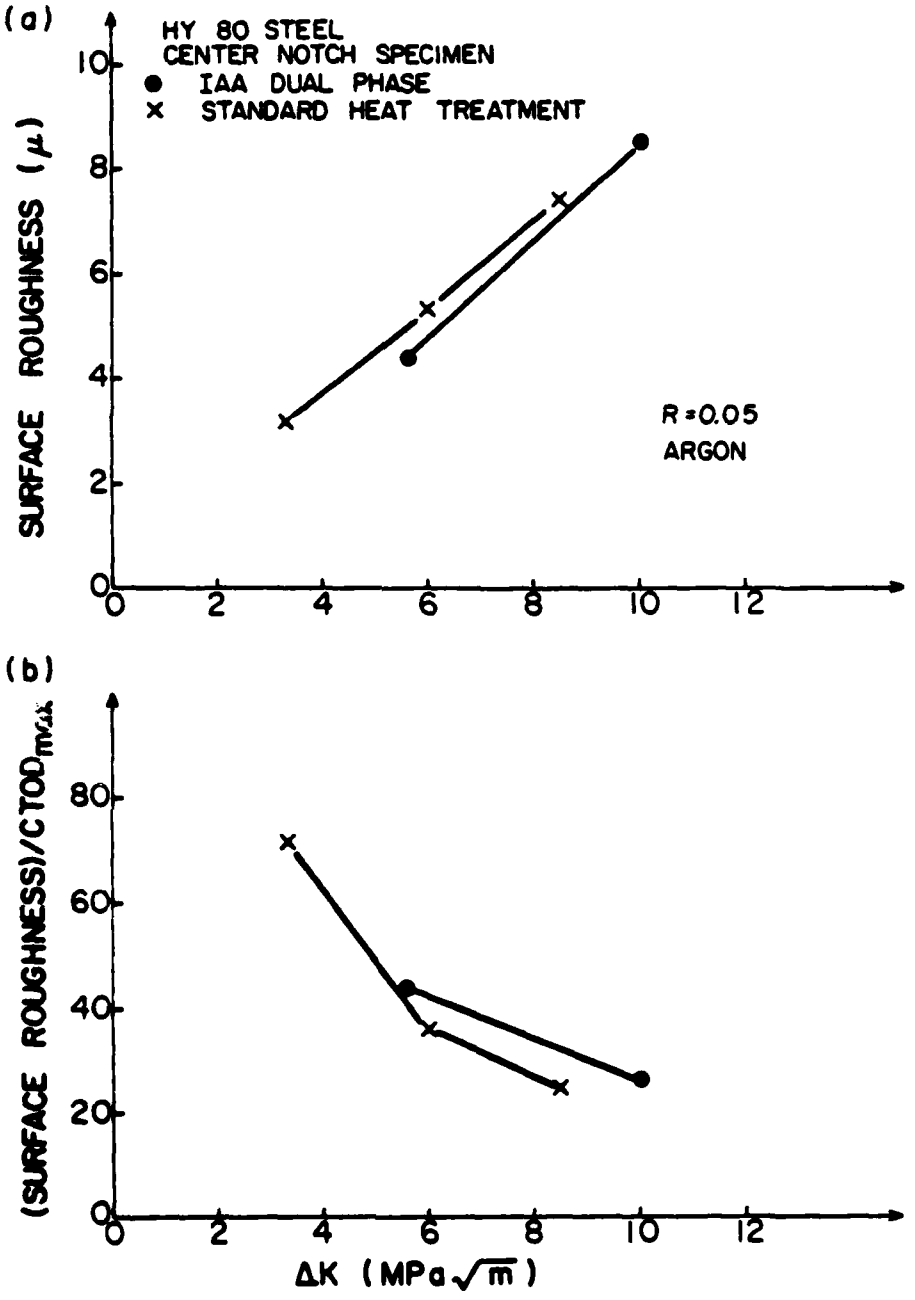

Figure 32. Comparison of the surface roughness behavior between the dual phase IAA and the standard heat treatment of HY80 steel.

(a) Surface roughness versus ΔK

(b) (Surface roughness)/$CTOD_{max}$ versus ΔK

can then be calculated from this equation. The results are shown in Table 10.

Table 10. HY130 Steel with Four Tempering Structures

	σ_y(0.2%) (MN/m^2)	ϵ_f* (%)	ΔK_{th} ($MN/m^{\frac{3}{2}}$)	ΔK_{T_3} ($MN/m^{\frac{3}{2}}$)	$\bar{\ell}$ (μm)
400° C, 10 hrs	1084	43.9	2.77	3.35	0.32
550° C, 5 hrs	1068	48.4	3.04	3.43	0.34
610° C, 1 hr	1033	50.3	3.59	3.98	0.49
650° C, $\frac{1}{4}$ hr	1033	46.0	3.16	3.72	0.43

* The result based on 0.3" gage section specimen.

From the magnitude of $\bar{\ell}$ and the observation of the microstructures by TEM (e.g., Fig. 3(c)), the value $\bar{\ell}$ is close to the lath martensite width rather than the carbide spacing. The results suggest that the morphology of the lath martensite may play an important role on the fatigue crack propagation resistance at low ΔKs. These results are also consistent with the results of Yoder et al.[22] for martensitic type steels. Tempering at higher temperature gives some beneficial effect since some lath martensites in as-quenched state can recover and grow to rather large sizes and relax to a lower dislocation density. As discussed in the previous section, s in Eq.(3) is a material parameter similar to $\bar{\ell}$ controlling fatigue crack propagation at low ΔK regime.

For HY80 steel, the transition stress intensity for the different heat treatments were also determined and $\bar{\ell}$ calculated. The results are shown in Table 11.

Comparing the two dual phase structures where the martensite phase acts as a strong barrier to fatigue crack propagation, the higher threshold value of the dual phase IAA compared IAB can be simply explained by the larger value of s in Eq.(3) since the larger prior austenite grain size should give

Table 11. HY80 Steel with Various Heat Treatments

	σ_y (MN/m^2)	Prior Austenite Grain Size (μm)	ΔK_{th} ($MN/m^{\frac{3}{2}}$)	ΔK_T ($MN/m^{\frac{3}{2}}$)	$\bar{\ell}$ (μm)
Dual Phase IAA	829	35	5.4	6.24	1.37
Dual Phase IAB	667	12	4.3	4.55	1.24
IAAT (650° C, 1 hr)	590	35	4.4	5.13	1.58
Standard Heat Treatment	638	12	3.1	3.45	0.98

larger martensite width which was confirmed by TEM observation. The same concept can also be used to explain why IAA followed by tempering (IAAT) still gives a higher threshold value and a higher closure stress level than the standard heat treatment. From Table 11, the ratio of the effective grain size of IAAT to the standard heat treatment (S.T.), $\bar{\ell}_{IAAT}/\bar{\ell}_{S.T.}$, is equal to 1.6. Since both IAAT and S.T. give similar strength levels (same hardness), α and σ_s in Eq.(3) to a first approximation are approximately the same. The grain size ratio s_{IAAT} to $s_{S.T.}$ is 2.0. The two ratios are thus only slightly different. This may suggest that s in Eq.(3) is related to the grain size. Further study to quantify α and σ_s is necessary.

SUMMARY AND CONCLUSIONS

1. The plastic work of fatigue crack propagation U for HY80 and HY130 steels with the standard heat treatments have been measured at the mid-ΔK of 20 MPa $\sqrt{m}$. U is much larger for HY80 than for HY130 in keeping with its lower fatigue crack propagation rate. The values of A in the equation $da/dN = A(\Delta K)^4/\mu\sigma_y' U$, Eq.(1), are essentially the same as found in other steels.

2. The tempering treatment in HY130 was varied keeping the strength

level constant to give four quite different microstructures. In the mid-ΔK range da/dN was almost the same for all. A small environmental effect was found when testing in laboratory air compared to dry argon atmosphere, with argon giving the lower rates. Thus in HY130, U seems to be independent of microstructure when strength level is kept constant.

3. The threshold fatigue crack propagation stress intensity range in HY80 and HY130 with standard heat treatments differ by only a small amount, 4.2 and 3.8 $MN/m^{\frac{3}{2}}$ respectively.

4. For the four different microstructures of HY130 referred to in conclusion 2, the highest threshold stress intensity value and the lowest fatigue crack propagation rate in the low ΔK region occurs with the standard heat treatment and correlates with the formation of the stable carbide (VC), increase in recovered lath martensite size and the lower dislocation density. The results are consistent with the equation $\Delta K_{th} = \alpha\sigma_s\sqrt{2\pi s}$, Eq.(3).

5. In HY80 steel two different dual phase steels with the ferrite phase isolated and surrounded by interconnected martensite were developed. As compared with the standard heat treatment, the dual phase structures improve the resistance to near-threshold fatigue crack propagation. Near the threshold ΔK fine shear lips occur in each structure; however, it is difficult to confirm that a shear fracture mode prevails because the spacing in the microstructure is comparable to the cyclic plastic zone size. The threshold value for each structure is proportional to the closure stress and surface roughness, but ΔK_{eff}^{th} also varies with heat treatment.

6. Using the Yoder et al. equation, the effective grain size was estimated from the yield strength and the transition stress intensity in HY80 and HY130 steels. This parameter appears to be related to s in Eq.(3).

Suitably increase the effective grain size without sacrificing the strength or ductility may be the route to improve the fatigue crack propagation resistance in the low ΔK region.

REFERENCES

1. S. Ikeda, Y. Izumi and M. E. Fine, Eng. Fract. Mech. 9, 123 (1977).
2. P. K. Liaw, S. I. Kwun and M. E. Fine, Met. Trans. 12A, 49 (1981).
3. M. E. Fine and D. L. Davidson, "Quantitative Measurement of Energy Associated with a Moving Fatigue Crack", Symposium on International Conference on Quantitative Measurement of Fatigue Damage, May 10-11, 1982, Dearborn, MI. ASTM Special Technical Publication (STP) in press.
4. J. Weertman, "Fatigue Crack Propagation Theories", Proc. of 1978 ASM Materials Science Seminar: Fatigue and Microstructure, p. 279, 14-15 October 1978, St. Louis, Missouri.
5. M. E. Fine, Met. Trans. 11A, 365 (1980).
6. J. McKittrick, P. K. Liaw, S. I. Kwun and M. E. Fine, Met. Trans. 12A, 1535 (1981).
7. E. Hornbogen and K. H. Zum Gahr, Acta Met. 24, 581 (1976).
8. J. Lindigkeit, A. Gysler, and G. Lutjering, Met. Trans. 12A, 1613 (1981).
9. H. Suzuki and A. J. McEvily, Met. Trans. 10A, 475 (1979); K. Minakawa and A. J. McEvily, Scripta Met. 15, 633 (1981).
10. S. I. Kwun and M. E. Fine, Fatigue of Eng. Materials and Stru. 3, 367 (1980).
11. J. M. Barsom, E. J. Imhof and S. T. Rolfe, Eng. Fract. Mech. 2, 301 (1971).
12. S. Ikeda, T. Sakai and M. E. Fine, J. Mater. Sci. 12, 675 (1977).
13. S. I. Kwun and R. A. Fournelle, Met. Trans. 13A, 393 (1982).
14. J. R. Rice, ASTM STP 415, p. 247 (1967).
15. Y. Izumi and M. E. Fine, Eng. Fract. Mech. 11, 791 (1979).
16. S. T. Rolfe and J. M. Barsom, "Fracture and Fatigue Control in Structures", Prentice-Hall, Englewood Cliffs, N. J., 1977.
17. M. E. Fine and R. O. Ritchie, "Fatigue-Crack Initiation and Near-Threshold Crack Growth", Proc. of 1978 ASM Materials Science Seminar: Fatigue and Microstructure, p. 245, 14-15 October 1978, St. Louis, Missouri.

18. P. N. Thielen, M. E. Fine and R. A. Fournelle, Acta Met. 24, 1 (1976).

19. D. A. Woodford and R. W. Stepien, Met. Trans. 11A, 1951 (1980).

20. D. Gan and J. Weertman, Eng. Fract. Mech. 15, 87 (1981).

21. A. Otsuka, K. Mori and T. Miyata, Eng. Fract. Mech. 7, 429 (1975).

22. G. R. Yoder, L. A. Cooley and T. W. Crooker, "A Critical Analysis of Grain-Size and Yield Strength Dependence of Near-Threshold Fatigue-Crack Growth in Steels", NRL Memorandum Report 4576, July 15, 1981.

PUBLICATIONS

1. S. I. Kwun and M. E. Fine, "Fatigue Macrocrack Growth in Tempered HY80, HY130, and 4140 Steels: Threshold and Mid-ΔK Range", Fatigue of Engineering Materials and Structures 3, 367 (1980).

2. P. K. Liaw, S. I. Kwun and M. E. Fine, "Plastic Work of Fatigue Crack Propagation in Steels and Aluminum Alloys", Met. Trans. 12A, 49 (1981). (Also supported by AFOSR).

3. J. L. Horng and M. E. Fine, "Effect of Tempering Temperature on Near-Threshold and Mid-ΔK Fatigue Crack Propagation Rate in HY130 Steel". In preparation.

4. J. L. Horng and M. E. Fine, "Threshold Stress Intensity of HY80 Steel with Dual Phase Microstructures". In preparation.

5. S. I. Kwun, D. H. Park, J. L. Horng, P. K. Liaw and M. E. Fine, "Threshold Stress Intensity of Iron and Some Steels for Specimens with Center and Side Notches". In preparation.